

Supporting Information

**Emergence of Circularly Polarized Luminescence from Achiral *o*-
Carborane-Based Molecules through Molecular Vibrations Coupled
with Intramolecular Charge Transfer in Solid States**

Junfeng Li,* Limin Zhang, Sijia Zhao, Yingjie Li, Tao Wang, Min Gao, Yuhang Deng, Shunan Shi
State Key Laboratory of Flexible Electronics (LoFE), School of Chemistry and Life Sciences,
Nanjing University of Posts & Telecommunications, 9 Wenyuan Road, Nanjing 210023, China

* E-mail: iamjfli@njupt.edu.cn

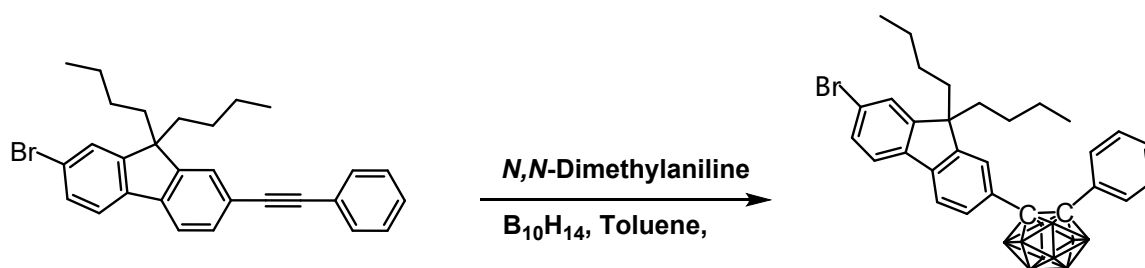
13. Instruments and materials

NMR spectra were recorded on a Bruker Ultra Shield Plus 400 MHz instrument with CDCl₃ as the solvent and tetramethylsilane (TMS) as the internal standard. UV-Vis spectra were obtained from a Perkin-Elmer Lambda 25 spectrometer. Fluorescent spectra were obtained with a 48000 DSCF spectrometer. Differential scanning calorimetry (DSC) profiles were measured on Netzsch DSC 200 F3. Thermo-gravimetric analysis (TGA) was performed on Shimadzu DTG-60A equipment. Time-resolved fluorescence decays were obtained from HORIBA JOBIN YVON Tem Pro-01 lifetime fluorescence spectroscopy. Absolute fluorescence/phosphorescence quantum yield was taken on Edinburgh Instruments' FLS980 fluorescence spectrophotometer attached with an integrating sphere. Raman spectroscopy was conducted on Horiba Labram Odyssey equipment. Single-crystal X-ray diffraction data collection and structure determination of *o*-1 and *o*-2 were performed at 295 K with an Xcalibur Onyx Nova four-circle diffractometer with a CCD system utilizing graphite-monochromatic Cu K α radiation ($\lambda = 1.54184 \text{ \AA}$). The empirical absorption correction was performed using the Crystal Clear program. The structure was solved using a direct method, and refined by full-matrix least-squares on F^2 employed in the program SHELXL-2016/6 program package. We employed the PLATON software/SQUEEZE subroutine to calculate the diffraction contribution of the solvent molecules and to generate a group of solvent-free diffraction intensities. The resulting new HKL file was used to further refine the structure. The crystallographic data and structure refinement parameters are summarized in Table S1-2, which contains the supplementary crystallographic data for this paper. *o*-1: CCDC numbers in 150 K, 240 K, and 298 K were 2184815, 2305916, and 2184817, respectively; *o*-2: CCDC numbers in 150 K, 220 K, and 298 K were 2184821, 2305917, and 2184823, respectively. These data can be obtained free of charge from The Cambridge

Crystallographic Data Centre. Circularly polarized luminescence (CPL) spectra were measured using a JASCO CPL-300 spectrofluoropolarimeter at room temperature. The instrument used a scattering angle of 0° from the excitation of unpolarized, monochromated incident light with a bandwidth of 10 nm. In order to keep the detector at the best state and obtain the precise signals, the DV values were monitored to about 0.5 V.

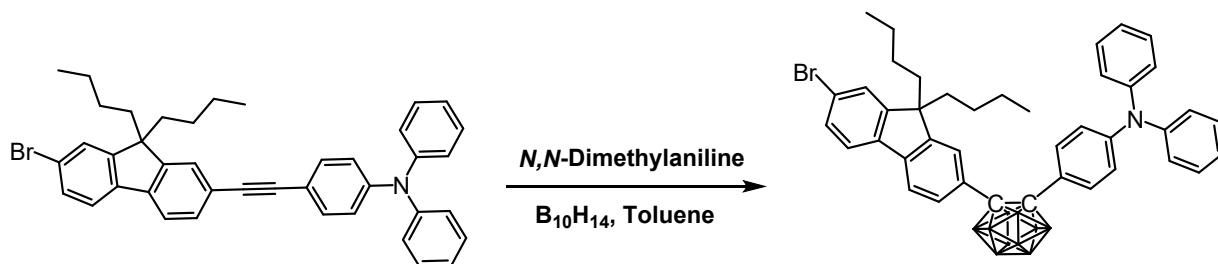
Toluene and THF were purified by distillation from sodium in the presence of benzophenone. Other chemicals were analytical grades and used without further purification.

14. Synthetic procedures and characterization



Synthesis of *o*-1: To a stirred toluene solution of decaborane ($B_{10}H_{14}$) (321.79 mg, 2.63 mmol) at room temperature was slowly added *N,N*'-dimethylaniline (637.60 mg, 5.26 mmol), and then refluxed for 2 h. After cooling down to 40 °C, 2-bromo-9,9-dibutyl-7-(phenylethynyl)-9H-fluorene (1.00 g, 2.19 mmol) was added in one portion and the final mixture was refluxed for 12 h. After being cooled to room temperature, the mixture was quenched by addition of methanol (20 mL). The organic phase was separated and the aqueous layer was extracted with CH_2Cl_2 (3×50 mL). The organic phases were combined, washed with brine, dried over anhydrous Na_2SO_4 , and concentrated in *vacuo*. The residual was purified by column chromatography on silica gel (gradient of petroleum ether (bp. 60-90 °C)/ CH_2Cl_2 , 90/10 to 30/10, v/v) to afford the title product as a white powder (758.26 mg, 60%). The white single crystal was obtained from CH_2Cl_2 /MeOH in 50% yield. 1H NMR (400 MHz, $CDCl_3$, δ /ppm): 7.40-7.32 (m, 7H), 7.26 (s, 1H), 7.09 (t, $J = 8$ Hz, 1H), 7.01 (t, $J = 8$ Hz, 2H), 1.79-1.68 (m,

4H), 0.98-0.86 (m, 4H), 0.57 (t, $J = 8$ Hz, 6H), 0.36-0.25 (m, 2H), 0.17-0.06 (m, 2H). ^{13}C NMR (101 MHz, CDCl_3 , δ/ppm): 152.37, 149.15, 140.95, 137.38, 129.68, 129.53, 129.18, 129.17, 129.13, 128.62, 127.12, 125.15, 123.89, 121.20, 120.62, 118.36, 85.00, 84.36, 54.31, 38.54, 24.54, 21.56, 12.79. ^{11}B NMR (128 MHz, CDCl_3 , δ/ppm): -2.67, -10.53.



Synthesis of *o-2*: To a stirred toluene solution of decaborane ($\text{B}_{10}\text{H}_{14}$) (234.85 mg, 1.92 mmol) at room temperature was slowly added *N,N'*-dimethylaniline (466.66 mg, 3.85 mmol), and then refluxed for 2 h. After cooling down to 40 °C, 4-((7-bromo-9,9-dibutyl-9H-fluoren-2-yl)ethynyl)-*N,N*-diphenylaniline (1.00 g, 1.60 mmol) was added in one portion and the final mixture was refluxed for 12 h. After being cooled to room temperature, the mixture was quenched by addition of methanol (20 mL). The organic phase was separated and the aqueous layer was extracted with CH_2Cl_2 (3 \times 50 mL). The organic phases were combined, washed with brine, dried over anhydrous Na_2SO_4 and concentrated in *vacuo*. The residual was purified by column chromatography on silica gel (gradient of petroleum ether (bp. 60-90 °C)/ CH_2Cl_2 , 95/5 to 80/20, v/v) to obtain the title product as a white powder (773.28 mg, 65%). The white single crystal was obtained from $\text{CH}_2\text{Cl}_2/\text{MeOH}$ in 75% yield. ^1H NMR (400 MHz, CDCl_3 , δ/ppm): 7.53 (d, $J = 8$ Hz, 1H), 7.49-7.43 (m, 4H), 7.38-7.36 (m, 1H), 7.19 (d, $J = 8$ Hz, 2H), 7.11 (t, $J = 8$ Hz, 4H), 7.00-6.97 (m, 2H), 6.87 (d, $J = 8$ Hz, 4H), 6.65 (d, $J = 8$ Hz, 2H), 1.95-1.82 (m, 4H), 0.99 (td, $J = 8$ Hz, 16 Hz, 4H), 0.60 (t, $J = 8$ Hz, 6H), 0.54-0.45 (m, 2H), 0.41-0.32 (m, 2H). ^{13}C NMR (101 MHz, CDCl_3 , δ/ppm): 153.57, 150.30, 149.33, 146.42, 141.92, 138.50, 131.40, 130.29, 129.75, 129.35, 126.36, 126.00, 125.23, 124.05, 122.88, 122.25,

121.54, 120.15, 119.03, 86.59, 86.45, 55.37, 39.63, 25.66, 22.75, 13.66. ^{11}B NMR (128 MHz, CDCl_3 , δ/ppm): -2.99, -11.14.

15. NMR spectra

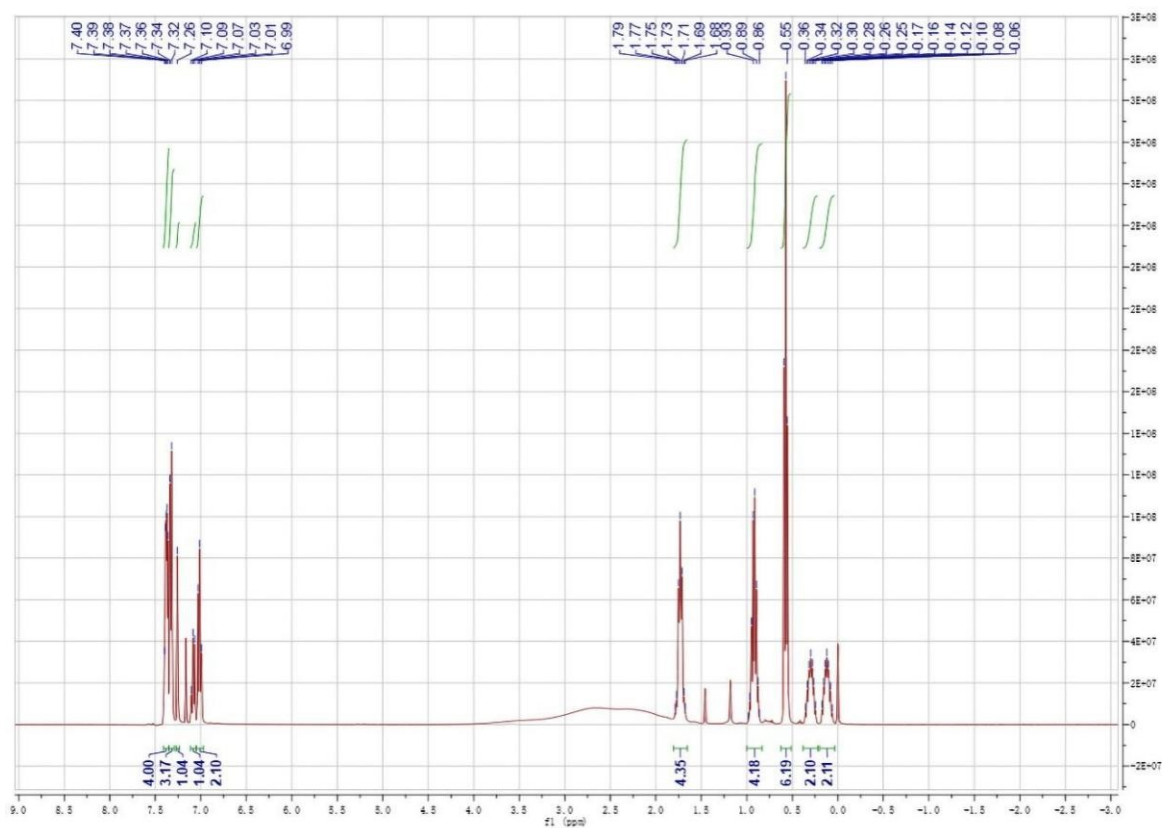


Figure S1. ^1H NMR spectra of *o*-1 in CDCl_3 solution.

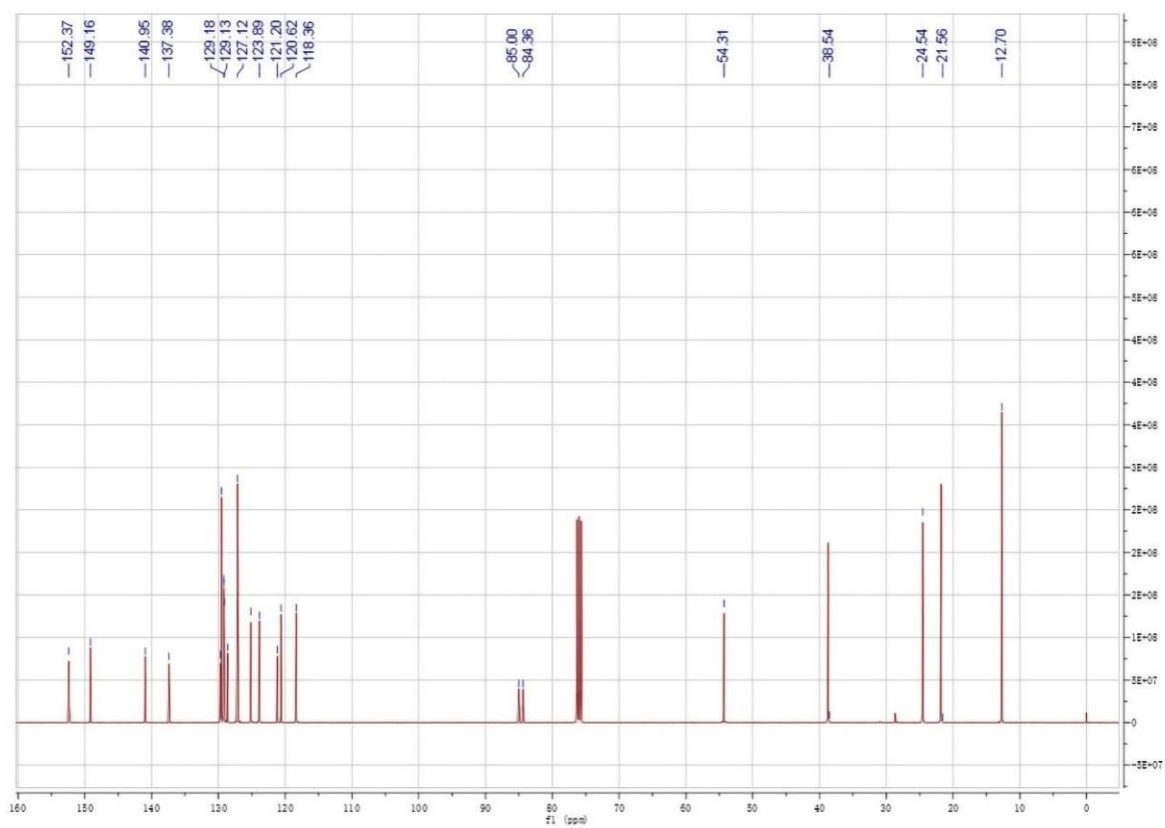


Figure S2. ^{13}C NMR spectra of *o*-1 in CDCl_3 solution.

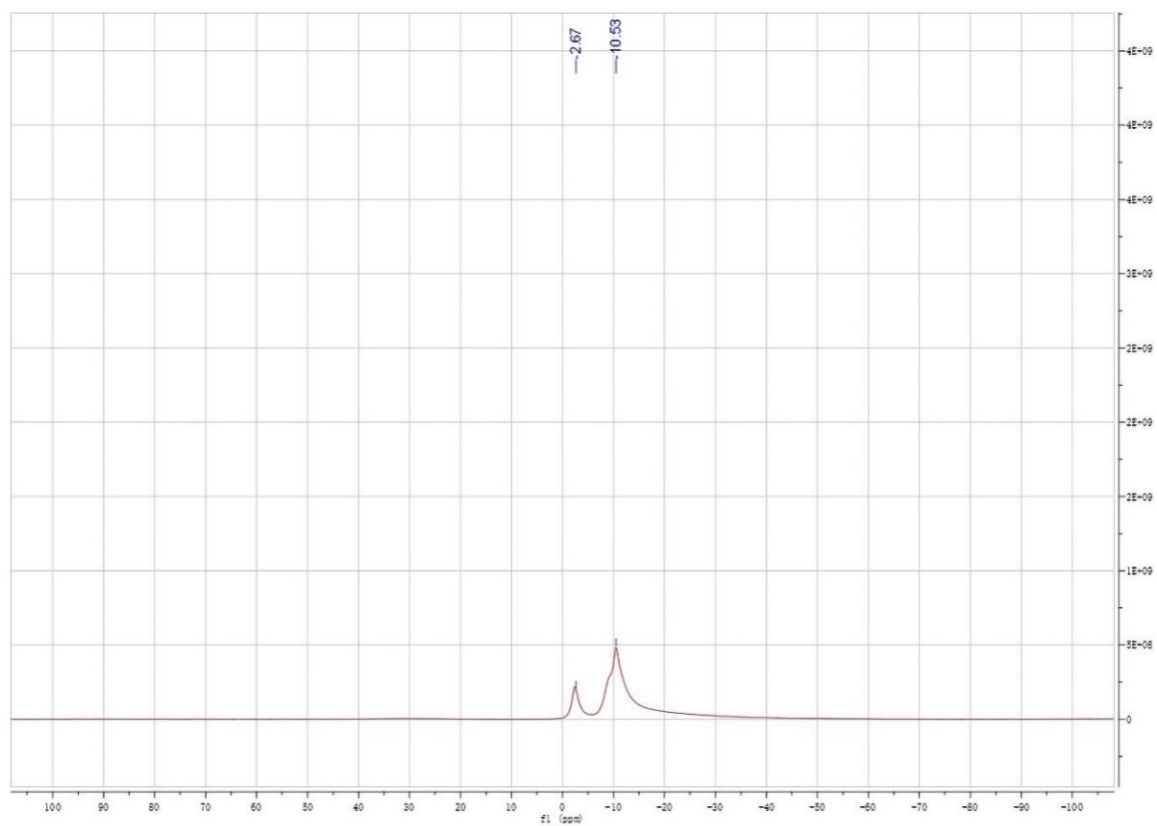


Figure S3. ^{11}B NMR spectra of *o*-1 in CDCl_3 solution.

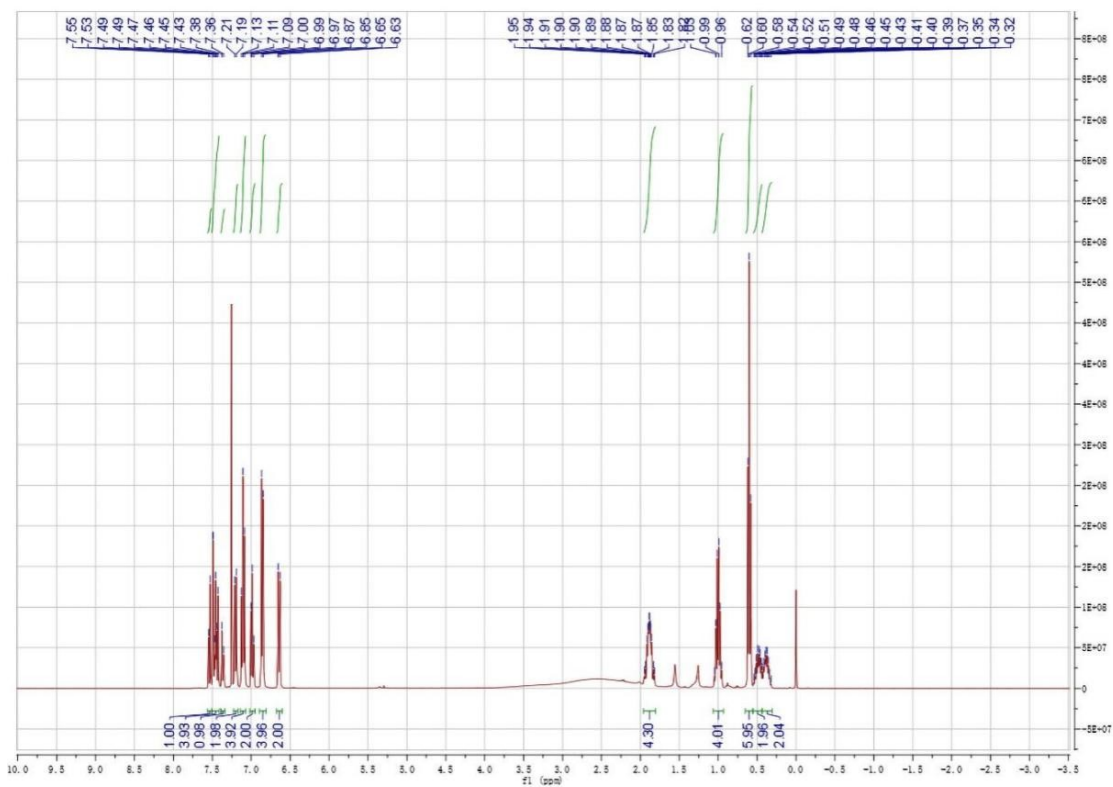


Figure S4. ^1H NMR spectra of *o*-2 in CDCl_3 solution.

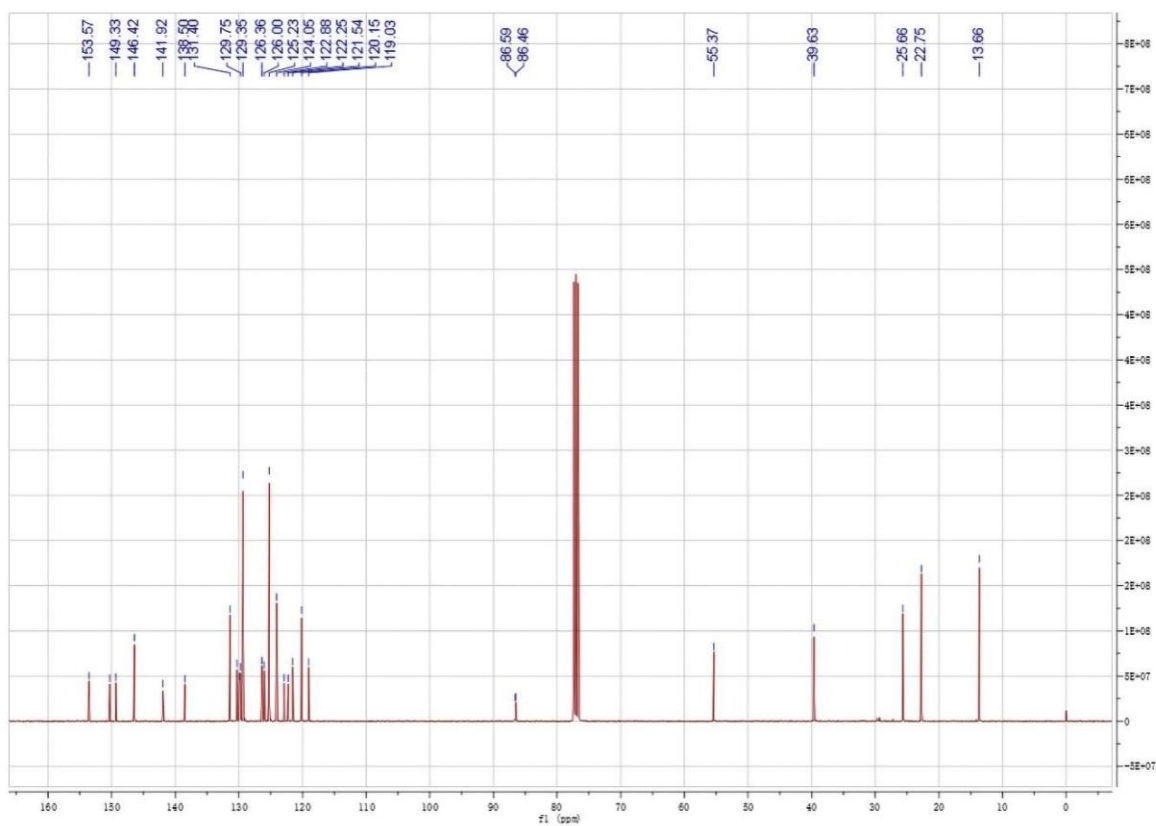


Figure S5. ^{13}C NMR spectra of *o*-2 in CDCl_3 solution.

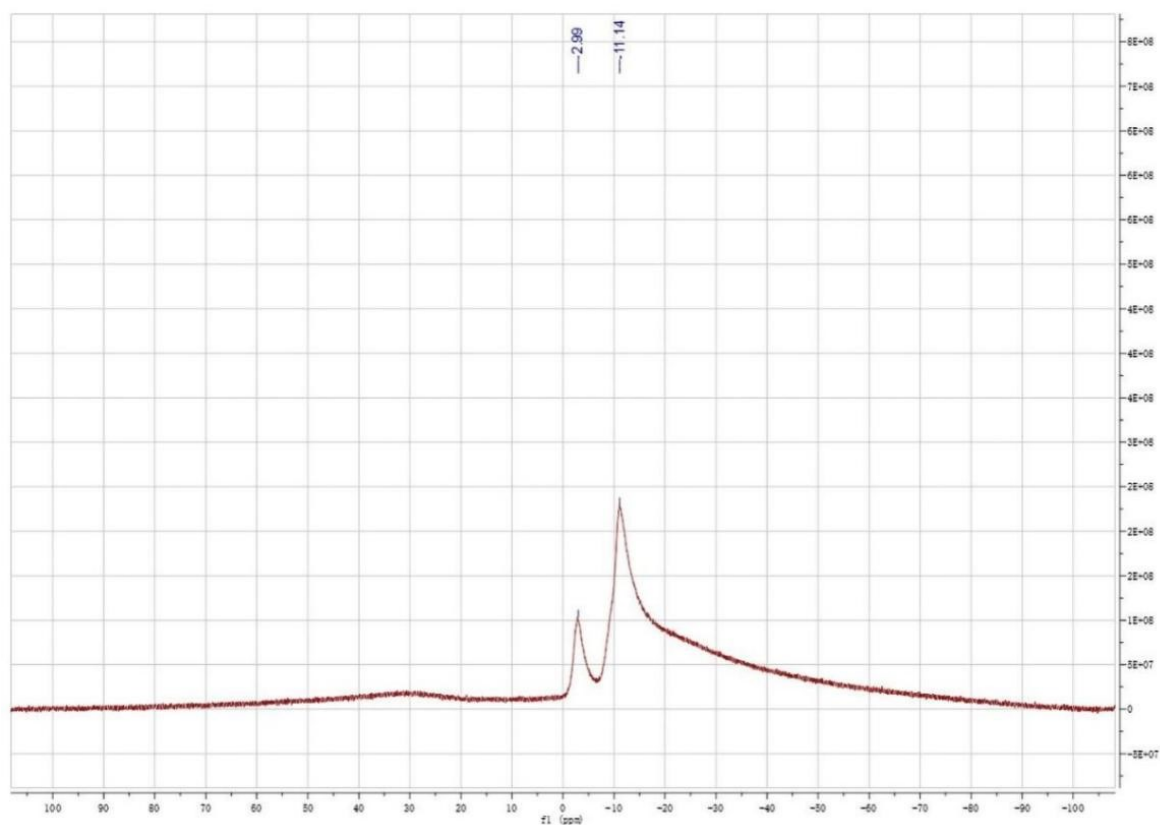


Figure S6. ^{11}B NMR spectra of **o-2** in CDCl_3 solution.

4. Thermo-gravimetric analysis

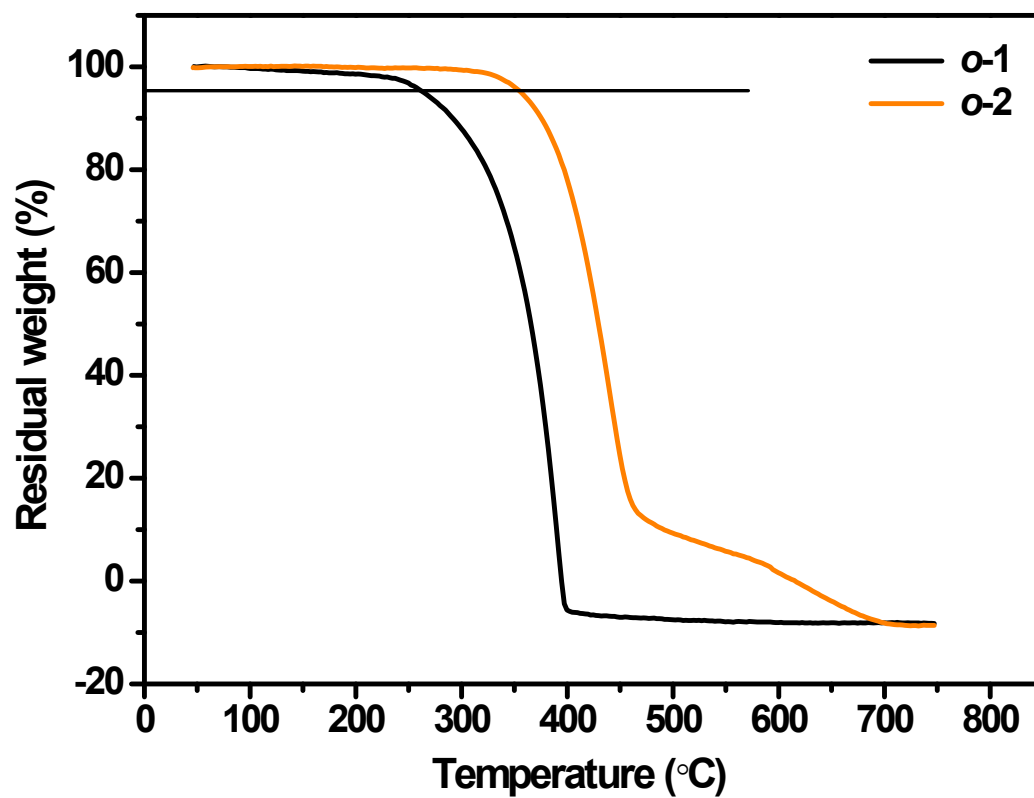


Figure S7. TGA profiles of the crystal ***o*-1** and ***o*-2** (Corresponding to the black bold line and orange bold line, respectively). The heating rate is 20 °C/min. There was no decrease in the weight percent of the samples until decomposition. These results indicated that both samples did not include solvent molecules in the crystals.

5. Aggregation-induced emission

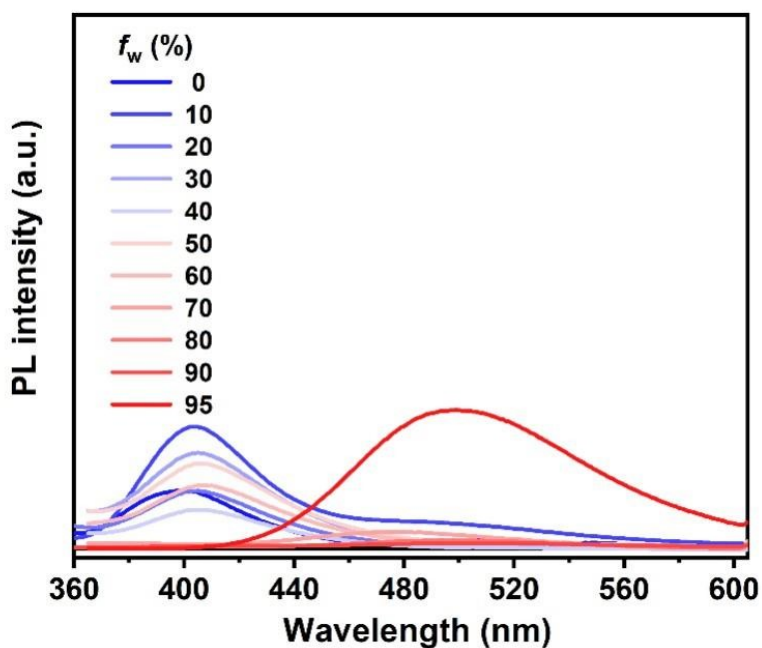


Figure S8. Emission spectra of ***o*-1** in THF, upon increasing the concentration of water from 0% to 95% with concentration of 10 μ M ($\lambda_{\text{ex}} = 320$ nm).

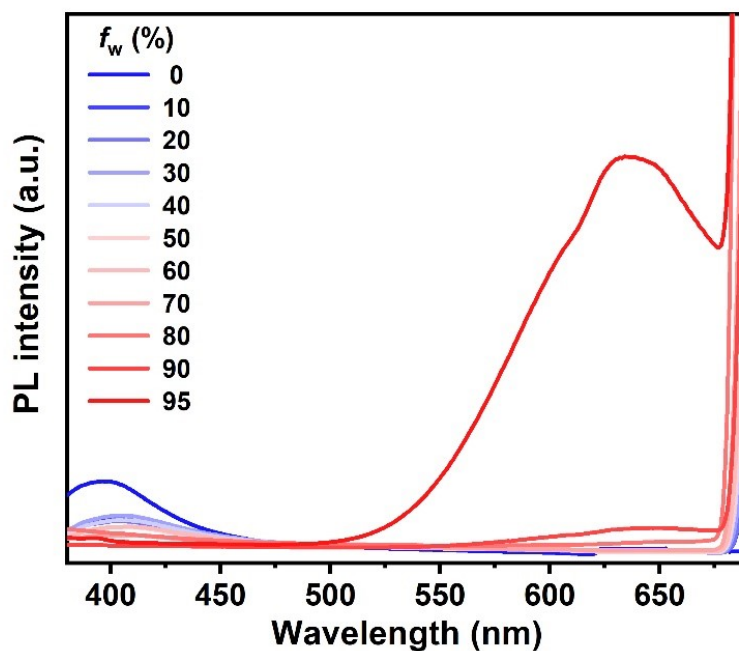


Figure S9. Emission spectra of *o*-2 in THF, upon increasing the concentration of water from 0% to 95% with concentration of 10 μ M ($\lambda_{\text{ex}} = 320$ nm).

6. Temperature-dependent UV-vis spectra in organic solvent

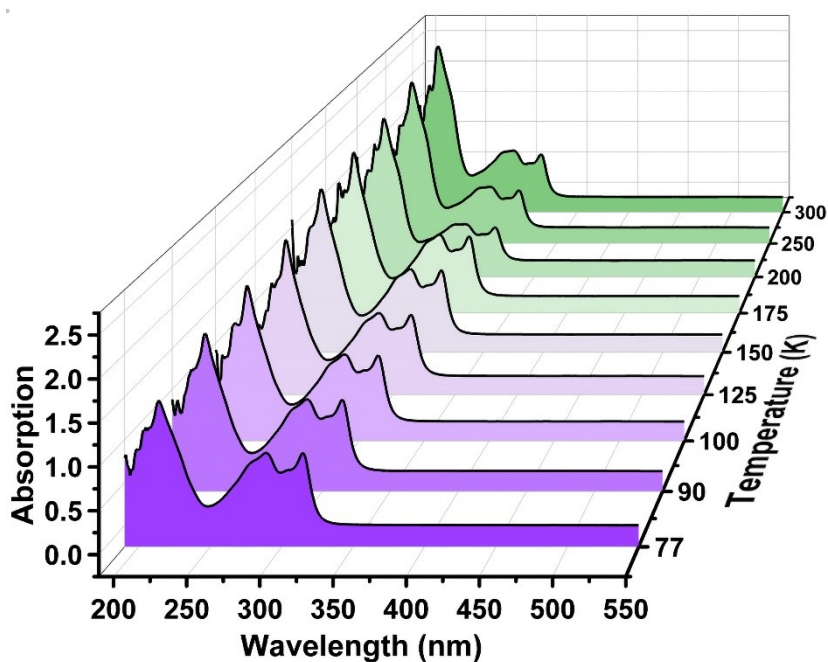


Figure S10. Temperature-dependent UV-vis spectra of *o*-1 in the 1-chlorobutane solvent with a concentration of 10 μ M (Temperature: 77 K, 90 K, 100 K, 125 K, 150 K, 175 K, 200 K, 250 K, 300 K).

K).

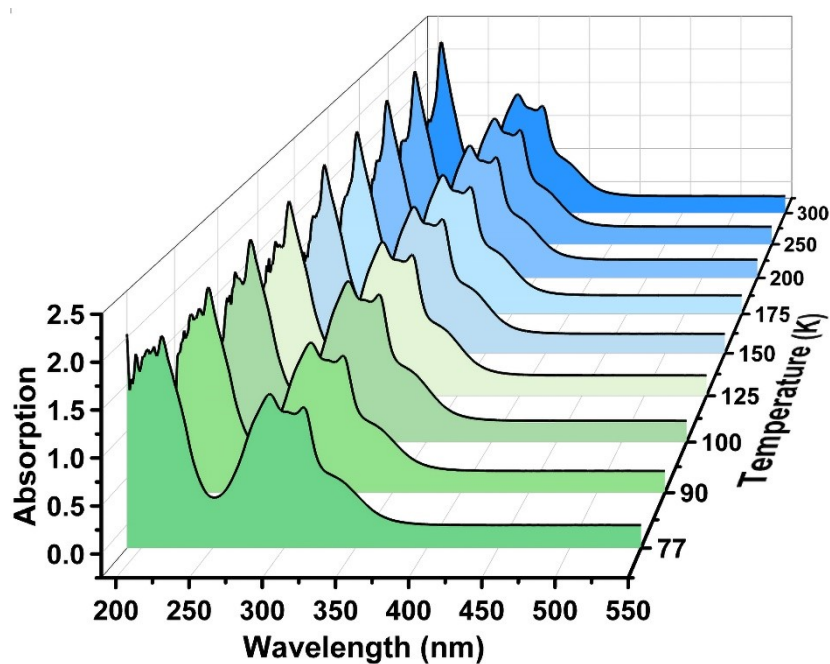


Figure S11. Temperature-dependent UV-vis spectra of *o*-2 in the 1-chlorobutane solvent with a concentration of 10 μM (Temperature: 77 K, 90 K, 100 K, 125 K, 150 K, 175 K, 200 K, 250 K, 300 K).

7. Temperature-dependent emission spectra in organic solvent

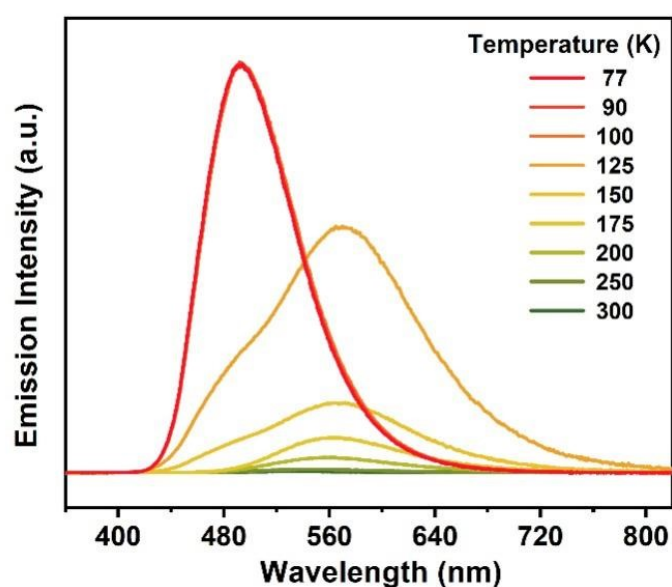


Figure S12. Temperature-dependent emission spectra of *o*-1 in the 1-chlorobutane solvent with a

concentration of 100 μM (Temperature: 77 K, 90 K, 100 K, 125 K, 150 K, 175 K, 200 K, 250 K, 300 K).

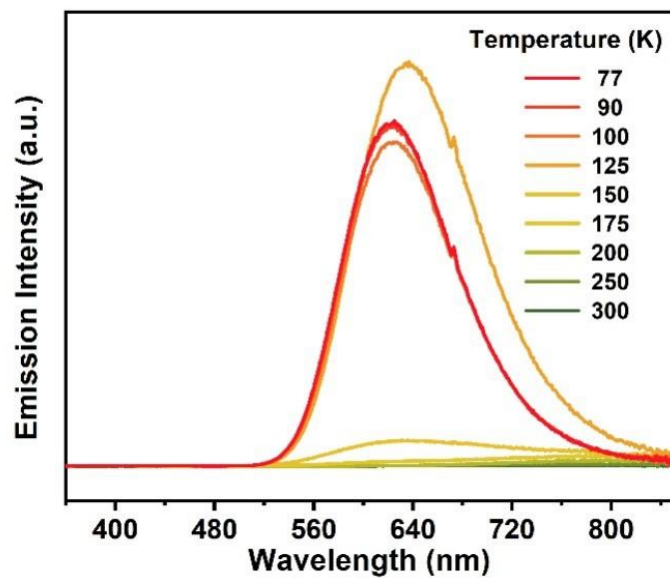


Figure S13. Temperature-dependent emission spectra of *o*-2 in the 1-chlorobutane solvent with a concentration of 100 μM (Temperature: 77 K, 90 K, 100 K, 125 K, 150 K, 175 K, 200 K, 250 K, 300 K).

8. Single crystal X-ray Diffraction

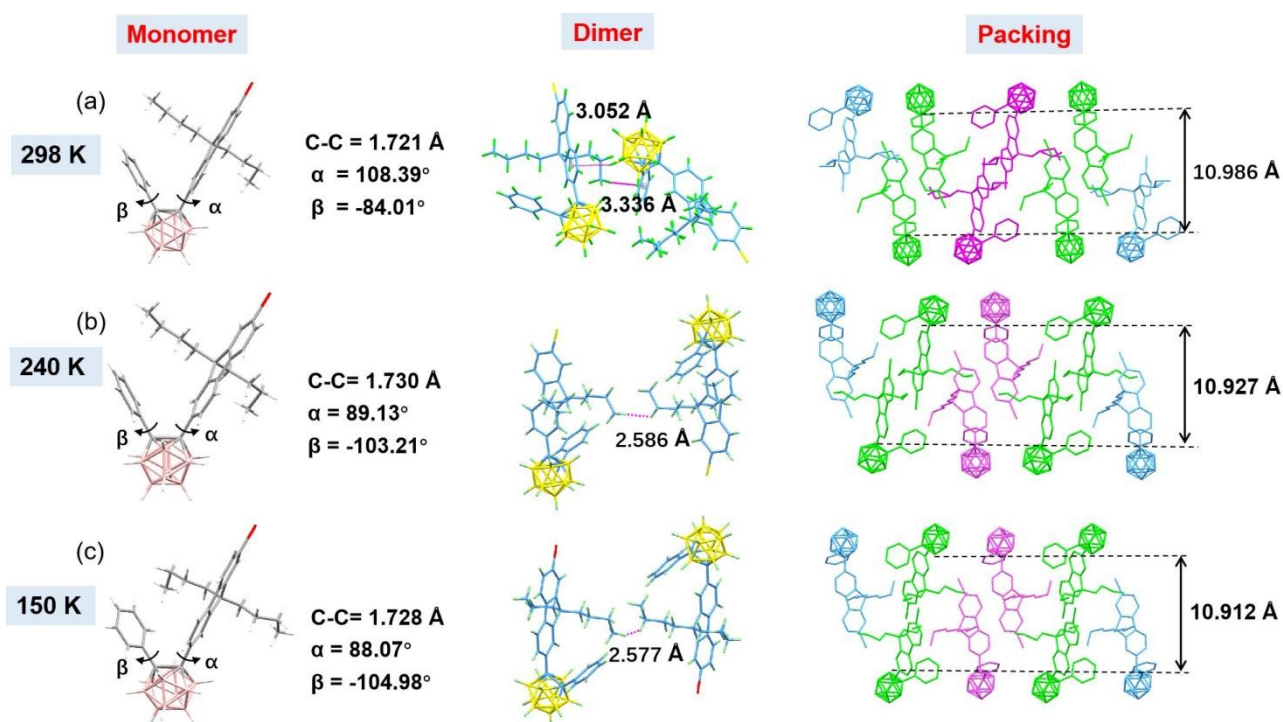


Figure 14. Crystal structure, intermolecular interactions, and molecular packing of *o*-1 at 150 K, 240 K, and 298 K, respectively.

Table S1. Crystal Data and Structure Refinement for *o*-1 at 150 K, 240 K, and 298 K, respectively.

Compound	<i>o</i> -1 at 150 K	<i>o</i> -1 at 240 K	<i>o</i> -1 at 298 K
Empirical Formula	C ₂₉ H ₃₉ B ₁₀ Br	C ₂₉ H ₃₉ B ₁₀ Br	C ₂₉ H ₃₉ B ₁₀ Br
Formula Weight	575.61	575.61	575.61
Temperature / K	150.00	240.00	298.00
Crystal System	triclinic	triclinic	triclinic
Space Group	P-1	P-1	P-1
a / Å	13.0497(3)	13.1415(7)	13.345(3)
b / Å	14.9599(3)	15.0389(9)	14.946(4)
c / Å	17.2358(4)	17.2174(10)	17.337(5)
α / °	78.2880(10)	79.399(4)	81.259(17)
β / °	68.0520(10)	68.401(3)	67.976(13)
γ / °	87.5960(10)	88.116(3)	88.943(14)
V / Å ³	3053.83(12)	3107.5(3)	3167.8(14)
Z	4	4	4
ρ _{calc} / g cm ⁻³	1.252	1.230	1.207
μ / mm ⁻¹	1.945	1.911	1.875
F (000)	1192.0	1192.0	1192.0
Crystal size/mm ³	0.15 × 0.13 × 0.12	0.13 × 0.11 × 0.1	0.14×0.13×0.11
Radiation Cu K _α	λ = 1.54178	λ = 1.54184	λ = 1.54184
2θ range for data collection / °	5.644 to 136.76	5.618 to 133.194	5.568 to 137.78
Index ranges	-13 ≤ h ≤ 15, -17 ≤ k ≤ 18, -20 ≤ l ≤ 20	-15 ≤ h ≤ 15, -17 ≤ k ≤ 17, -20 ≤ l ≤ 20	-14 ≤ h ≤ 16, -18 ≤ k ≤ 18, -20 ≤ l ≤ 20
Reflections collected	107453	35130	29419
Independent reflections	11193	10751	11583
	R _{int} = 0.0358	R _{int} = 0.0367	R _{int} = 0.0317
	R _{sigma} = 0.0198	R _{sigma} = 0.0334	R _{sigma} = 0.0369
Data/restraints/parameters	11193/0/725	10751/307/800	11583/0/764
Goodness-of-fit on F ₂	1.005	1.057	1.064
Final R indexes [I ≥ 2σ (I)]	R ₁ = 0.0288	R ₁ = 0.0428	R ₁ = 0.0512
	ωR ₂ = 0.0776	wR ₂ = 0.1088	ωR ₂ = 0.01412
Final R indexes [all data]	R ₁ = 0.0288	R ₁ = 0.0531	R ₁ = 0.0703
	ωR ₂ = 0.0776	wR ₂ = 0.1163	ωR ₂ = 0.1571
Largest diff. peak/hole / e Å ⁻³	0.57/-0.58	0.55/-0.64	0.33/-0.60

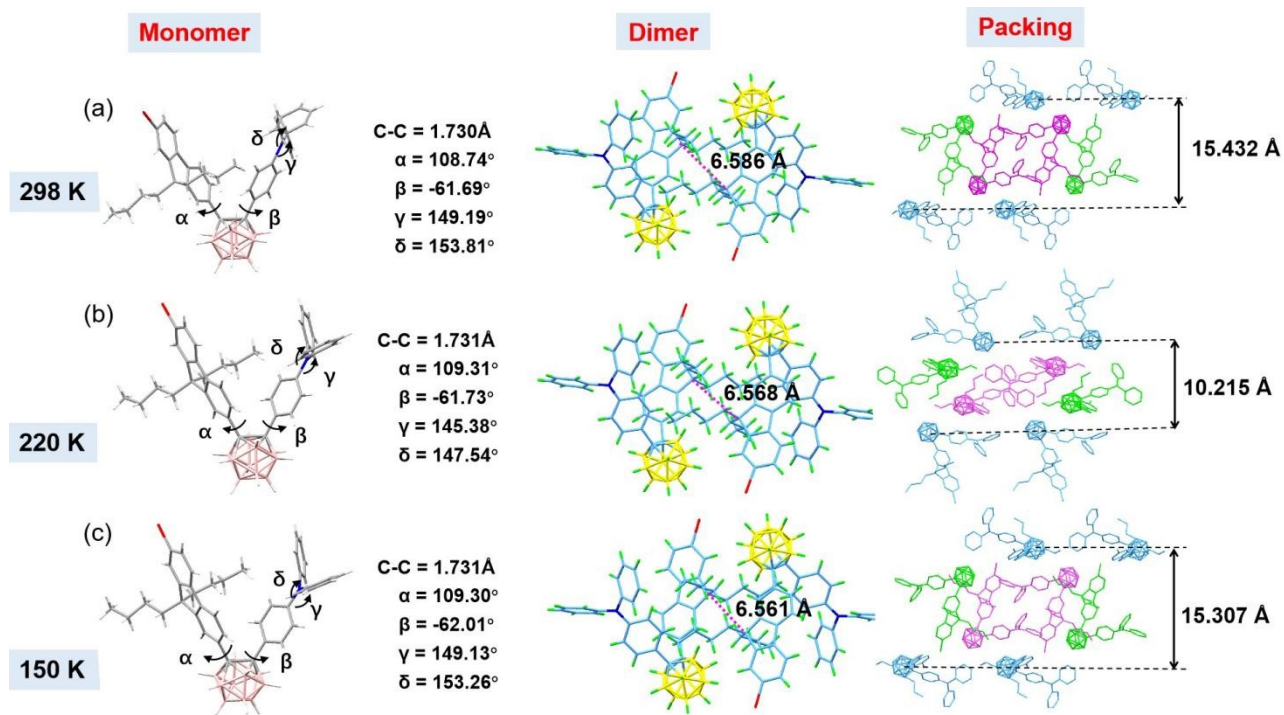


Figure S15. Crystal structures, intermolecular interactions, and molecular packing of *o*-2 at 150 K, 220 K, and 298 K, respectively.

Table S2. Crystal Data and Structure Refinement for *o*-2 at 150 K, 220 K and 298 K respectively.

Compound	<i>o</i> -2 at 150 K	<i>o</i> -2 at 220 K	<i>o</i> -2 at 298 K
Empirical Formula	C ₄₁ H ₄₈ B ₁₀ BrN	C ₄₁ H ₄₈ B ₁₀ BrN	C ₄₁ H ₄₈ B ₁₀ BrN
Formula Weight	742.81	742.81	742.81
Temperature / K	150.00	220.00	298.00
Crystal System	monoclinic	monoclinic	monoclinic
Space Group	P2 ₁ /n	P2 ₁ /n	P2 ₁ /n
a / Å	13.8599(4)	13.9749(4)	14.1406(13)
b / Å	20.3173(7)	20.3579(7)	20.4176(18)
c / Å	15.3748(5)	15.3992(5)	15.4246(14)
α / °	90	90	90
β / °	113.375(2)	113.6500(10)	114.323(4)
γ / °	90	90	90
V / Å ³	3974.1(2)	4013.1(2)	4058.1(6)
Z	4	4	4
ρ _{calc} / g cm ⁻³	1.241	1.229	1.216
μ/mm ⁻¹	1.621	1.605	1.587
F (000)	1544.0	1544.0	1544.0
Crystal size/mm ³	0.16 × 0.13 × 0.12	0.13 × 0.11 × 0.1	0.16 × 0.13 × 0.12
Radiation Cu K _α	λ = 1.54178	λ = 1.54184	λ = 1.54178
2θ range for data collection/ °	7.278 to 136.532	7.228 to 136.494	7.146 to 137.072
Index ranges	-15 ≤ h ≤ 16, -24 ≤ k ≤ 22, -18 ≤ l ≤ 18	-16 ≤ h ≤ 16, -22 ≤ k ≤ 23, -18 ≤ l ≤ 17	-16 ≤ h ≤ 17, -18 ≤ k ≤ 24, -18 ≤ l ≤ 18
Reflections collected	30811	35087	35869
Independent reflections	7242	7299	7386
	R _{int} =0.0286 R _{sigma} = 0.0240	R _{int} = 0.0384 R _{sigma} = 0.0280	R _{int} =0.0379 R _{sigma} = 0.0276
Data/restraints/parameters	7242/0/480	7299/912/588	7386/0/480
Goodness-of-fit on F ₂	1.039	1.037	1.079
Final R indexes [I ≥ 2σ (I)]	R ₁ = 0.0284	R ₁ = 0.0327	R ₁ = 0.0437
	ωR ₂ = 0.0751	wR ₂ = 0.0844	ωR ₂ = 0.01203
Final R indexes [all data]	R ₁ = 0.0306	R ₁ = 0.0392	R ₁ = 0.0534
	ωR ₂ = 0.0765	wR ₂ = 0.0886	ωR ₂ = 0.1280
Largest diff. peak/hole / e Å ⁻³	0.29/-0.43	0.26/-0.52	0.49/-0.55

9. Differential Scanning Calorimetry (DSC)

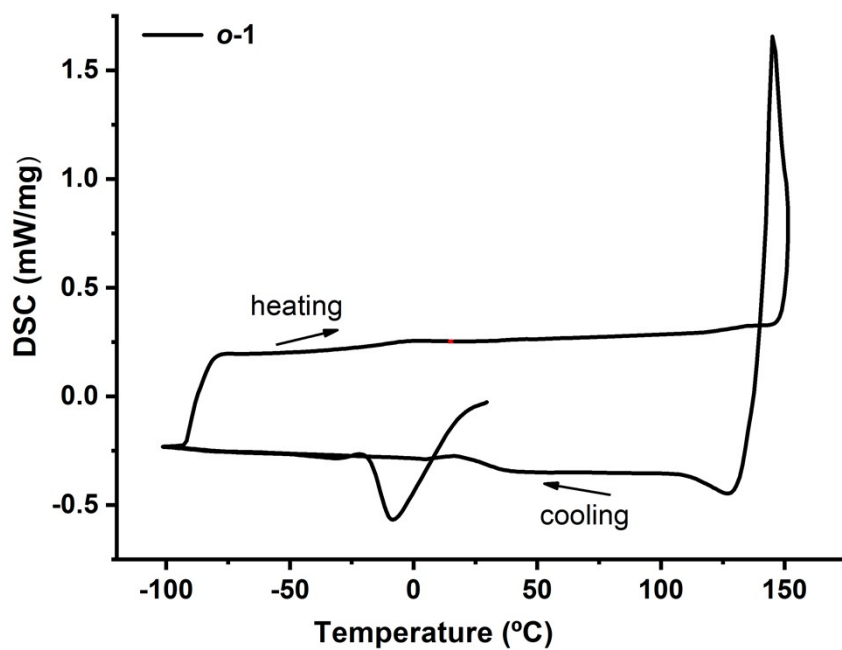


Figure S16. DSC profiles of crystal *o*-1. Heating and cooling rates were 10 °C /min, respectively.

There were no exo- or endo-thermic peaks in both crystalline samples.

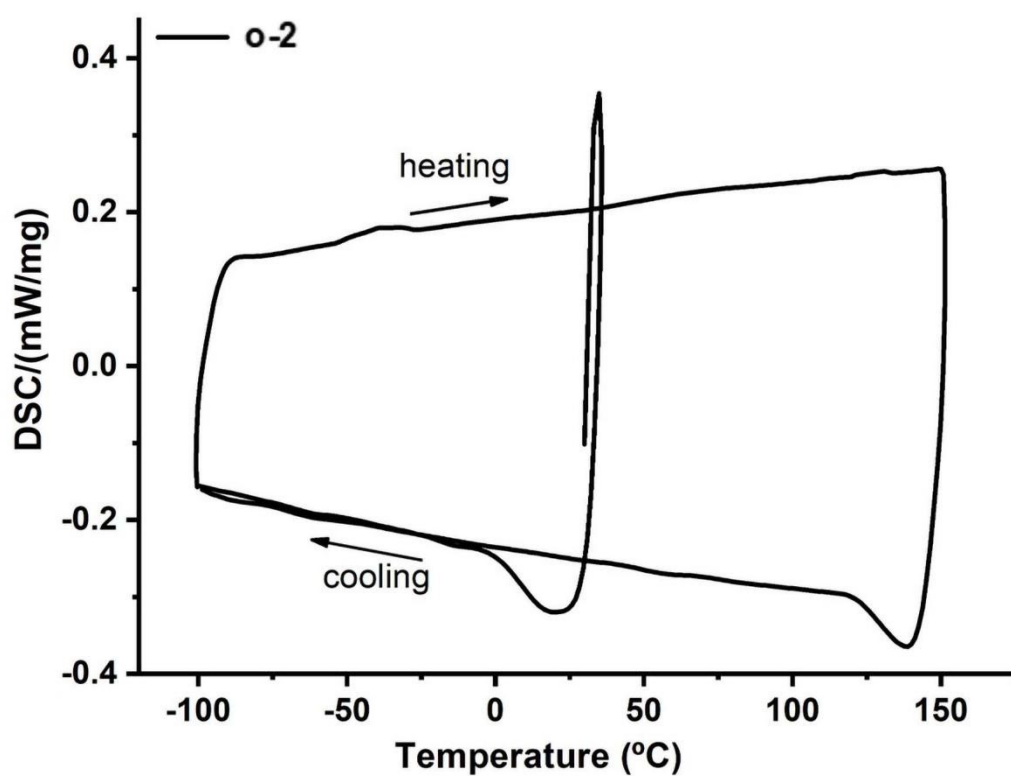


Figure S17. DSC profiles of crystal *o*-2. Heating and cooling rates were 10 °C /min, respectively.

There were exo- or endo-thermic peaks in both crystalline samples.

10. UV-vis spectra in solid states

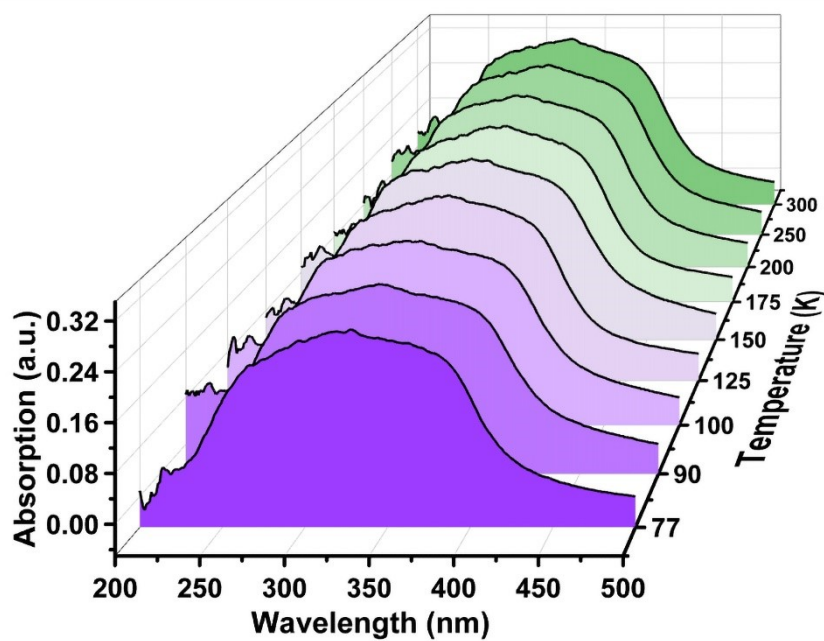


Figure S18. UV-Vis spectra of *o-1* in the solid states responding to various temperatures, including 77 K, 90 K, 100 K, 125 K, 150 K, 175 K, 200 K, 250 K, 300 K.

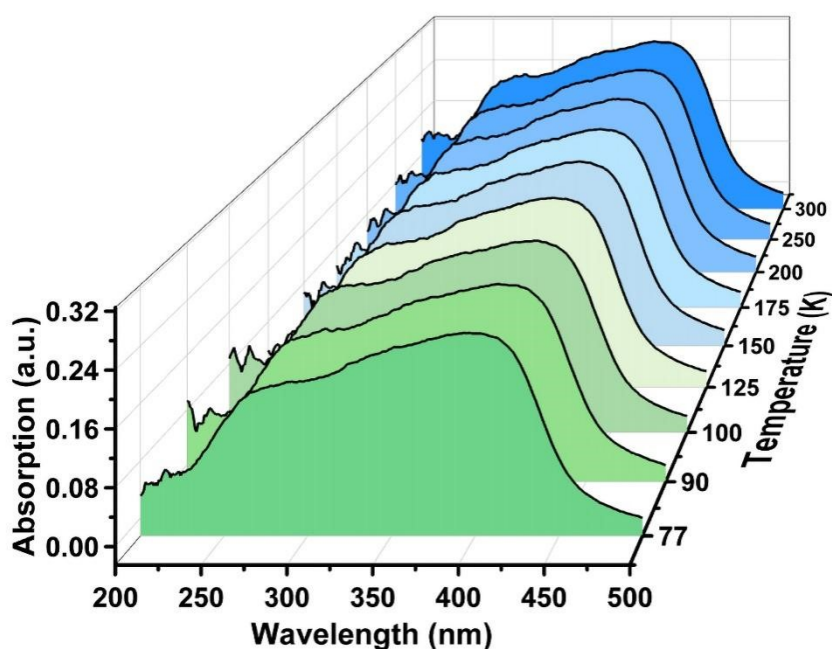


Figure S19. UV-Vis spectra of *o-2* in the solid states responding to various temperatures, including 77 K, 90 K, 100 K, 125 K, 150 K, 175 K, 200 K, 250 K, 300 K.

11. Analysis of fluorescence and phosphorescence

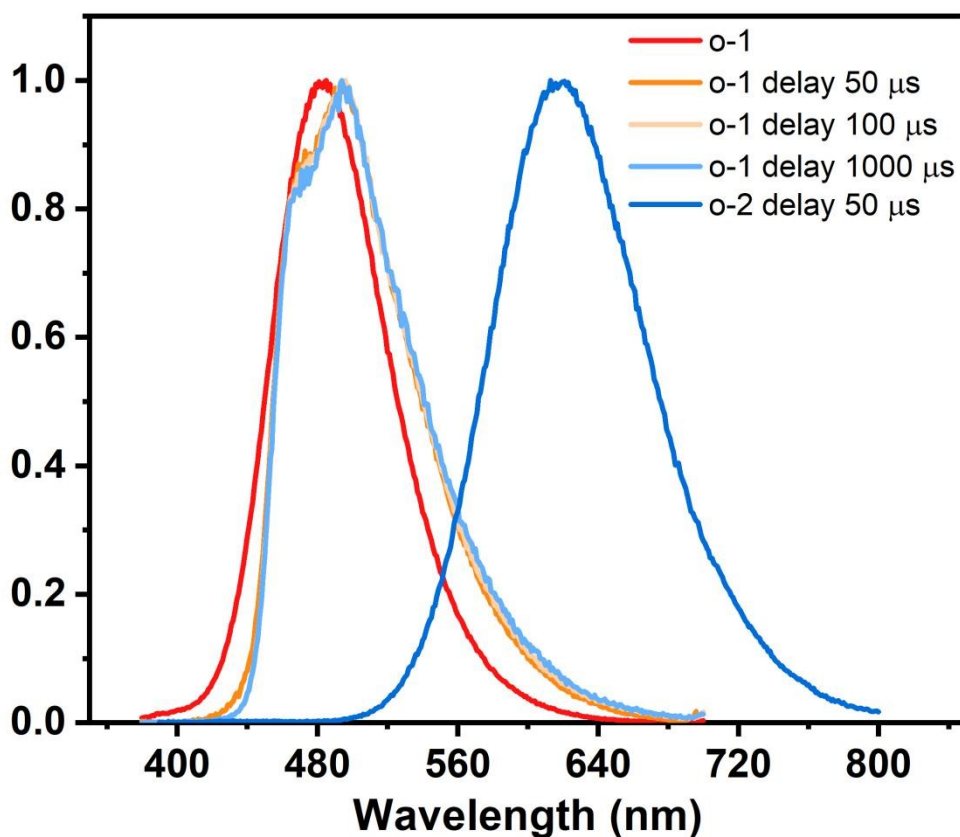


Figure S20. Delayed emissions of *o*-1 and *o*-2 in the crystal states at different time-gated windows.

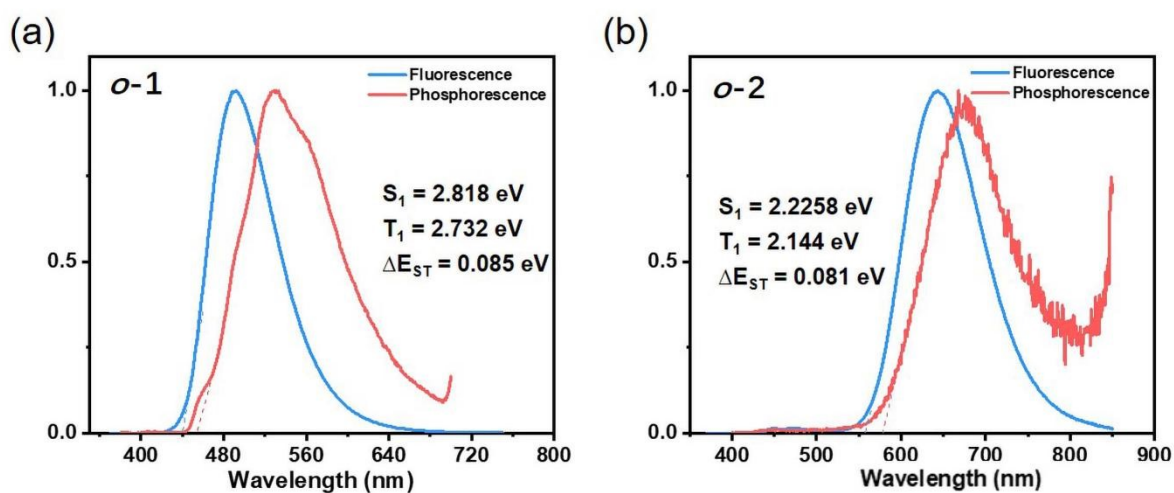


Figure S21. Prompt and delayed emission spectra *o*-1 and *o*-2 in the crystal states at 77 K, $\lambda_{\text{exc}} = 350$ nm.

12. Theoretical calculations

We determined the vertical excitation energy of *o*-carborane-based molecules by optimizing their molecular structures extracted from various crystal structures using the Gaussian16 program package.¹ Molecular structure optimization was performed at the PBE0/6-311G(d) level through Density Functional Theory (DFT) calculations. Vertical excitation calculations were carried out at the TD-PBE0/def2-tzvp level. To enhance the accuracy of the excited state energy levels, we examined the potential energy surface of their triplet electronic states using Tamm-Dancoff Approximation density functional theory (TDA-DFT) with the PBE0/6-311G(d) functional. The transition density of these molecules was visualized and analyzed using Multiwfn 3.3.8 (dev) and VMD software.² The electron density functional theory (DFT) calculations have been carried out by the latest version of ORCA quantum chemistry software³ (Version 5.0.1). The Spin-Orbit Coupling (SOC) calculations were performed with PBE0 functional and the def2-tzvp basis set. SOC calculation was performed by spin-orbit mean-field (SOMF) method.⁴

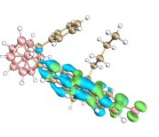
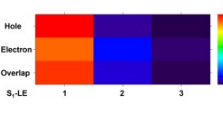
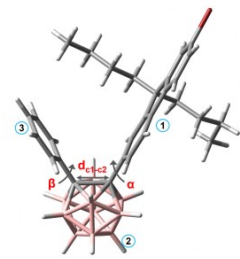
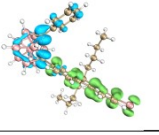
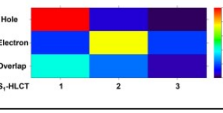
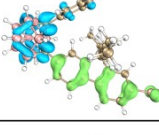
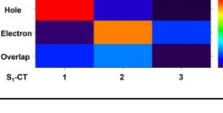
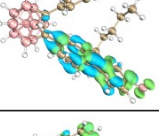
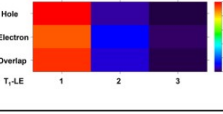
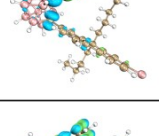
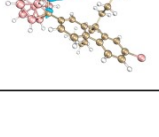
		Blue: Electron Green: Hole	RMSD		Electron	Hole	
S₁ LE 	LE LE(82.71%) CT(17.29%)		0.320 Å	 Hole: 0.956, 0.764, 0.573, 0.382, 0.191, 0.000 Electron: 0.956, 0.764, 0.573, 0.382, 0.191, 0.000 Overlap: 0.956, 0.764, 0.573, 0.382, 0.191, 0.000 S ₁ -LE	①:86.05% ②:11.77% ③: 2.18%	①:95.56% ②:4.00% ③:0.44%	①:Bromine-Fluorene ②:Carborane ③:Benzene ring 
	HLCT LE(18.69%) CT(81.31%)		0.271 Å	 Hole: 0.920, 0.736, 0.552, 0.368, 0.184, 0.000 Electron: 0.920, 0.736, 0.552, 0.368, 0.184, 0.000 Overlap: 0.920, 0.736, 0.552, 0.368, 0.184, 0.000 S ₁ -HLCT	①:15.18% ②:68.54% ③:16.28%	①:92.04% ②:6.55% ③:1.41%	
	CT LE(7.40%) CT(92.60%)		2.371 Å	 Hole: 0.934, 0.747, 0.560, 0.374, 0.187, 0.000 Electron: 0.934, 0.747, 0.560, 0.374, 0.187, 0.000 Overlap: 0.934, 0.747, 0.560, 0.374, 0.187, 0.000 S ₁ -CT	①:2.18% ②:81.83% ③:15.99%	①:93.41% ②:6.54% ③:0.05%	
T₁	LE LE(83.81%) CT(16.20%)		0.300 Å	 Hole: 0.955, 0.764, 0.573, 0.382, 0.191, 0.000 Electron: 0.955, 0.764, 0.573, 0.382, 0.191, 0.000 Overlap: 0.955, 0.764, 0.573, 0.382, 0.191, 0.000 T ₁ -LE	①:87.23% ②:11.06% ③:1.70%	①:95.53% ②:4.18% ③:0.29%	
T₂	HLCT LE(31.43%) CT(68.57%)		0.312 Å	 Hole: 0.649, 0.519, 0.389, 0.260, 0.130, 0.000 Electron: 0.649, 0.519, 0.389, 0.260, 0.130, 0.000 Overlap: 0.649, 0.519, 0.389, 0.260, 0.130, 0.000 T ₂ -HLCT	①:15.45% ②:56.51% ③:28.03%	①:16.09% ②:19.02% ③:64.89%	
T₃	LE LE(57.56%) CT(42.44%)		0.849 Å	 Hole: 0.785, 0.636, 0.477, 0.316, 0.159, 0.000 Electron: 0.785, 0.636, 0.477, 0.316, 0.159, 0.000 Overlap: 0.785, 0.636, 0.477, 0.316, 0.159, 0.000 T ₃ -LE	①:10.85% ②:20.55% ③:68.60%	①:12.41% ②:8.06% ③:79.53%	

Figure S22. The singlet electron density distributions (*isovalue* = 0.02) of LE, HLCT, and CT states for *o*-1 were calculated at the TD-PBE0/def2-tzvp levels by TD-DFT at the optimized S₀ geometry in the gas phase. The triplet electron density distributions (*isovalue* = 0.02) of T₁, T₂ and T₃ were calculated at TDA-PBE0/6-311G(d) levels using TD-DFT at the optimized S₀ geometry in the gas phase. The root-meansquare deviation (RMSD) analysis for different excited states (LE, HLCT, CT, T₁, T₂, and T₃). “Heat maps” of hole-electron analysis, and transferred electrons of paired fragments for *o*-1. Quantitative analysis of charge transfer for LE, HLCT, CT, T₁, T₂, and T₃ states.

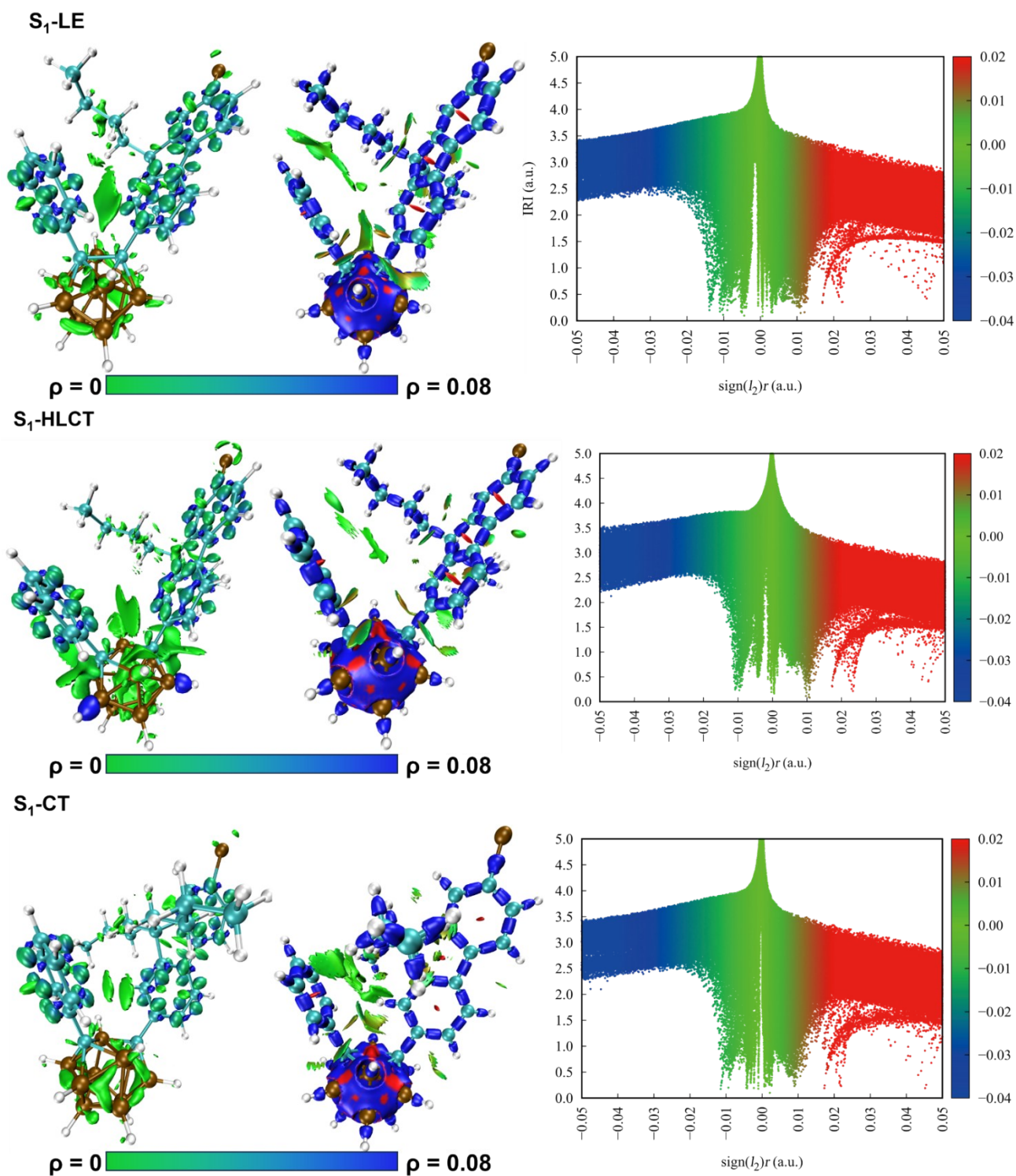
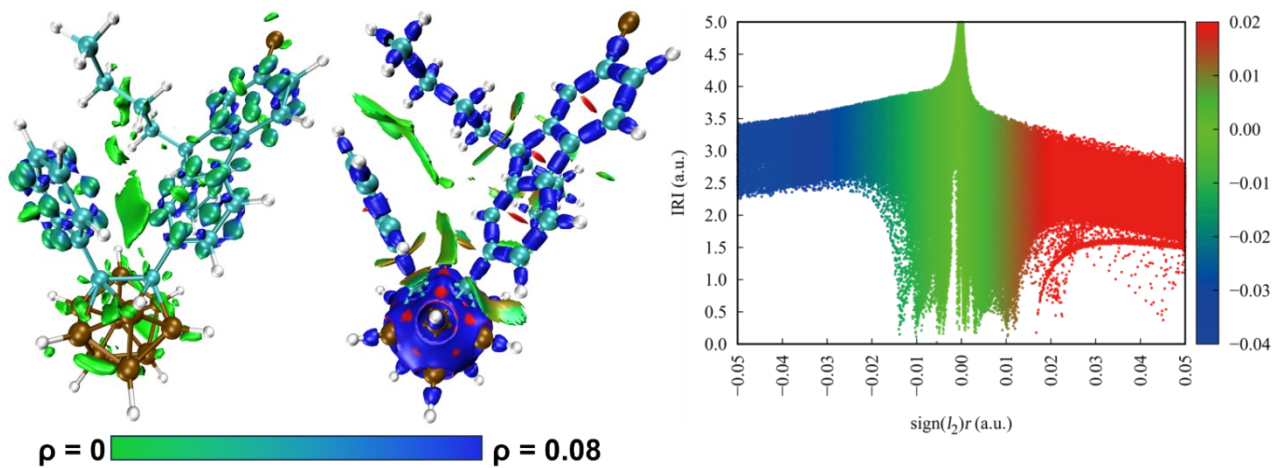


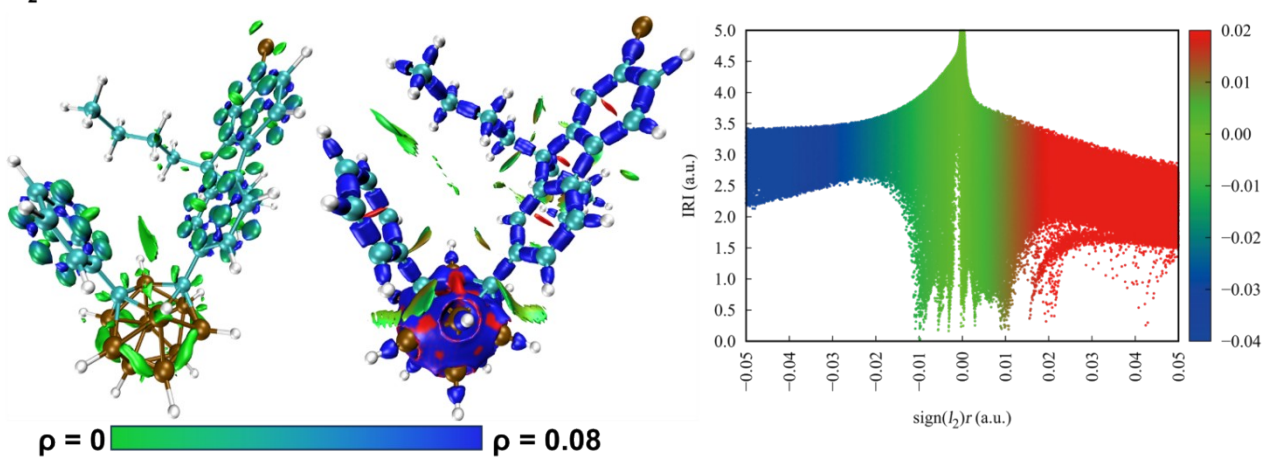
Figure S23. *IRI*- π isosurface (isovalue = 0.6) of **o-1** showing the π interactions between intramolecular interactions in the LE, HLCT, and CT states. *IRI* isosurfaces (isovalue = 0.6) of **o-1** in the LE, HLCT, and CT states showing the weak intramolecular interactions. Blue and green isosurfaces represent the covalent interactions and weak interactions, respectively. Plots of *IRI* vs the

electron density (ρ) of LE, HLCT, and CT states multiplied by the sign of the second Hessian eigenvalue (λ_2).

T₁-LE



T₂-HLCT



T₃-HLCT

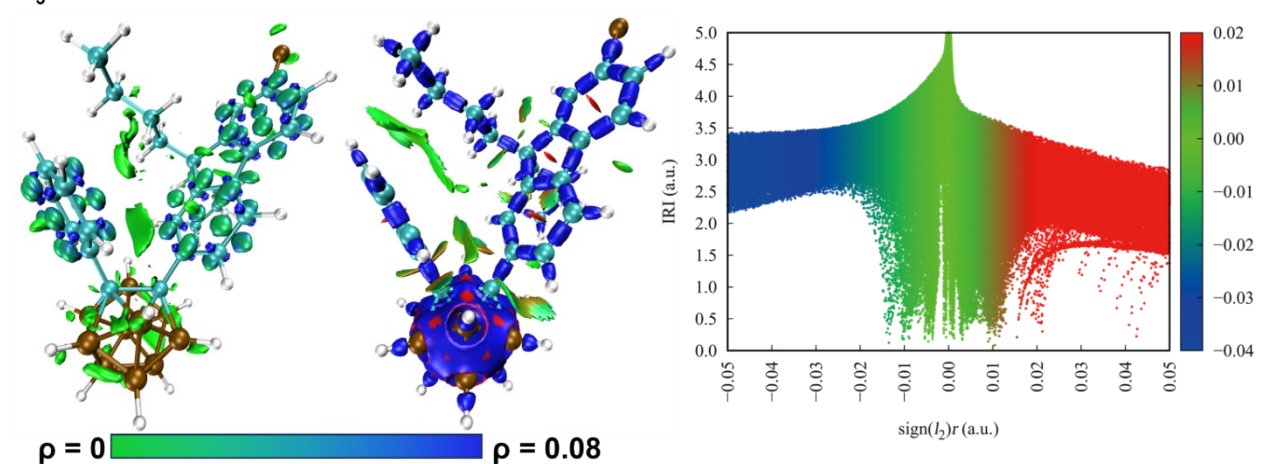


Figure S24. IRI- π isosurface (isovalue = 0.6) of ***o*-1** showing the π interactions between intramolecular interactions in the T₁, T₂, and T₃ states. IRI isosurfaces (isovalue = 0.6) of ***o*-1** in the

T₁, T₂, and T₃ states showing the weak intramolecular interactions. Blue and green isosurfaces represent the covalent interactions and weak interactions, respectively. Plots of IRI vs the electron density (ρ) of T₁, T₂, and T₃ states multiplied by the sign of the second Hessian eigenvalue (λ_2).

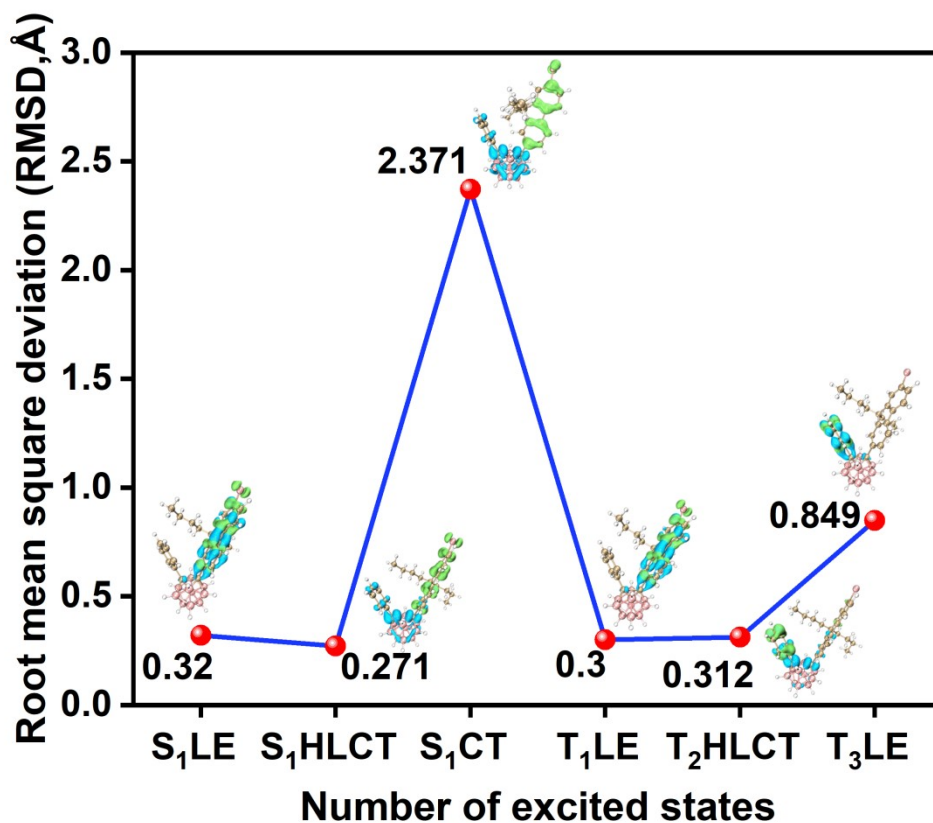


Figure S25. Analysis of root-meansquare deviation (RMSD) vs the different excited structures involved the LE, HLCT, CT, T₁, T₂, and T₃ states for *o-1*.

		Blue: Electron Green: Hole	RMSD		Electron	Hole	
S₁	CT LE(10.14%) CT(89.86%)		0.817 Å		①:30.99% ②:60.44% ③:8.56%	①:0.62% ②:2.77% ③:96.61%	 ①: Bromine-Fluorene ②: Carborane ③: Triphenylamine
S₂	HLCT LE(27.07%) CT(72.93%)		0.359 Å		①:60.94% ②:2.57% ③:27.48%	①:0.62% ②:2.77% ③:96.61%	
T₁	HLCT LE(23.93%) CT(76.07%)		0.472 Å		①:22.75% ②:56.55% ③:20.70%	①:3.94% ②:8.78% ③:87.28%	
T₂	HLCT LE(44.58%) CT(55.42%)		0.644 Å		①:60.37% ②:32.34% ③:7.29%	①:66.76% ②:7.41% ③:25.83%	
T₃	LE LE(67.58%) CT(32.42%)		0.612 Å		①:17.72% ②:12.51% ③:69.77%	①:1.51% ②:2.77% ③:96.08%	

Figure S26. The singlet electron density distributions (*isovalue* = 0.02) of S₁ and S₂ states for *o-2* were calculated at the TD-PBE0/def2-tzvp levels using TD-DFT at the optimized S₀ geometry in the gas phase. The triplet electron density distributions (*isovalue* = 0.02) of T₁, T₂ and T₃ were calculated at TDA-PBE0/6-311G(d) levels using TD-DFT at the optimized S₀ geometry in the gas phase. The root-mean-square deviation (RMSD) analysis for different excited structures (S₁, S₂, T₁, T₂, and T₃). “Heat maps” of hole-electron analysis, and transferred electrons of paired fragments for *o-2*. Quantitative analysis of charge transfer for S₁, S₂, T₁, T₂, and T₃ states.

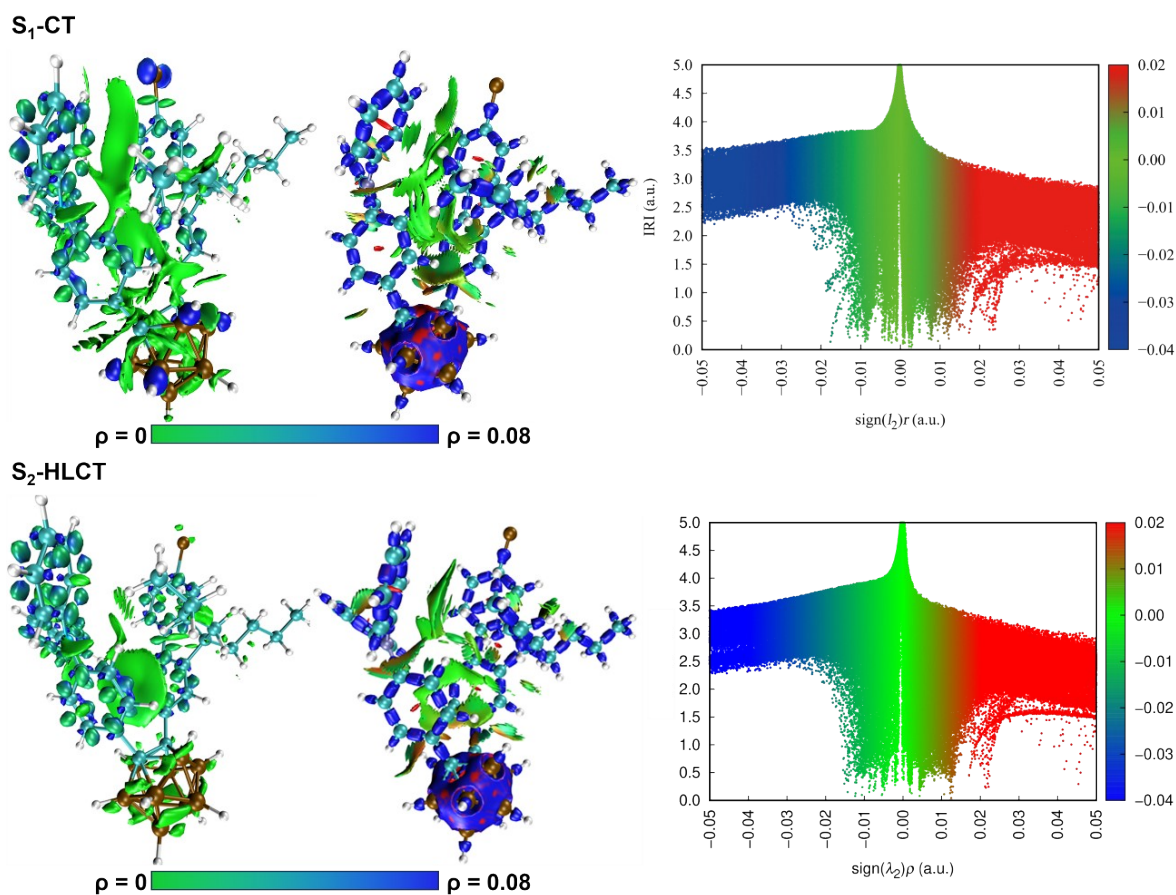
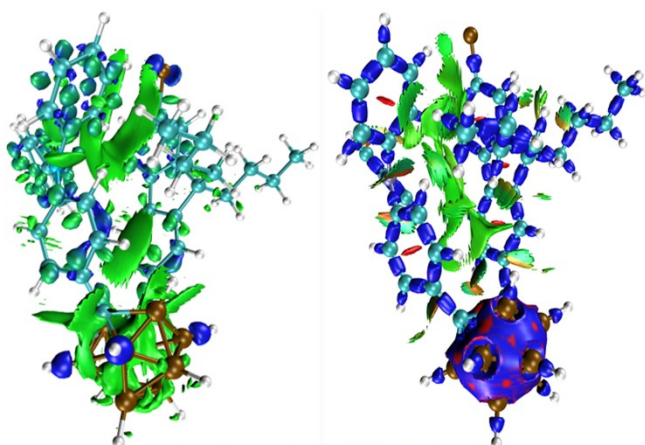
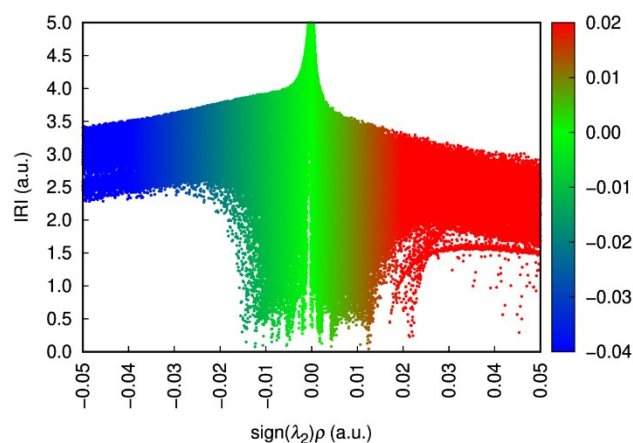


Figure S27. *IRI*- π isosurface (*isovalue* = 0.6) of *o*-2 showing the π interactions between intramolecular interactions in the S₁ and S₂ states. *IRI* isosurfaces (*isovalue* = 0.6) of *o*-2 in the S₁ and S₂ states showing the weak intramolecular interactions. Blue and green isosurfaces represent the covalent interactions and weak interactions, respectively. Plots of *IRI* vs the electron density (ρ) of S₁ and S₂ states multiplied by the sign of the second Hessian eigenvalue (λ_2).

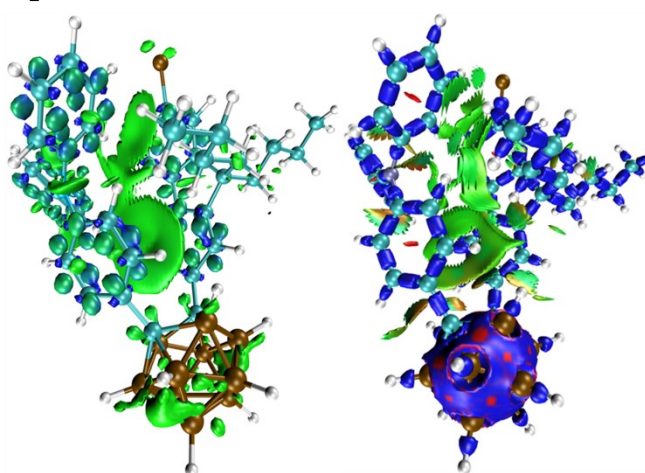
T₁-HLCT



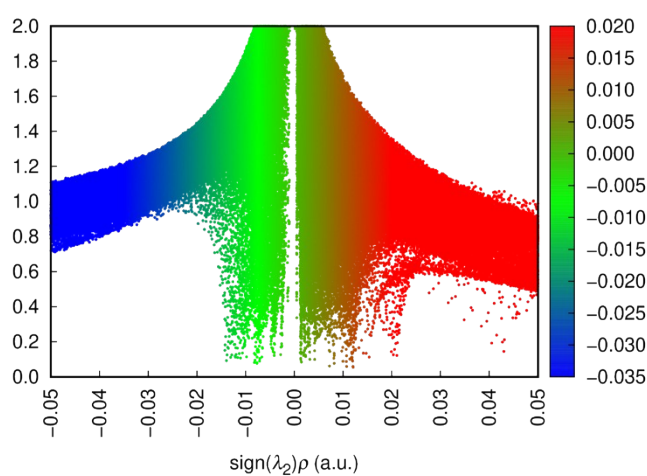
$\rho = 0$ $\rho = 0.08$



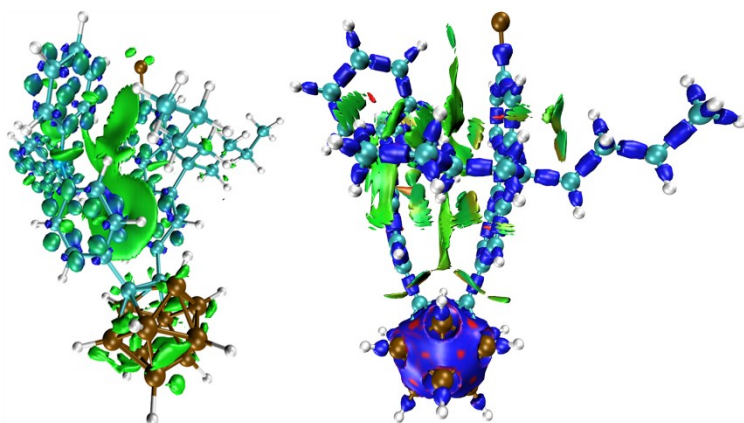
T₂-HLCT



$\rho = 0$ $\rho = 0.08$



T₃-LE



$\rho = 0$ $\rho = 0.08$

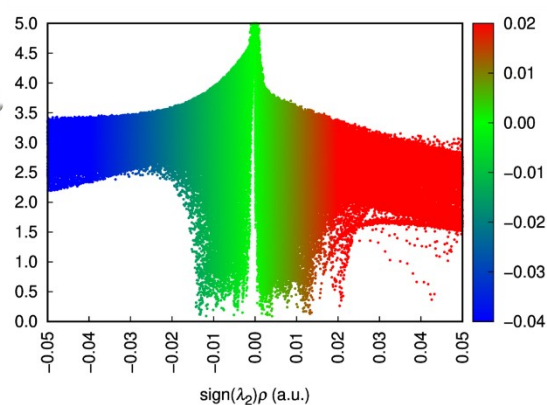


Figure S28. *IRI*- π isosurface (*isovalue* = 0.6) of *o*-2 showing the π interactions between intramolecular interactions in the T₁, T₂, and T₃ states. *IRI* isosurfaces (*isovalue* = 0.6) of *o*-2 in the T₁, T₂, and T₃ states showing the weak intramolecular interactions. Blue and green isosurfaces

represent the covalent interactions and weak interactions, respectively. Plots of IRI vs the electron density (ρ) of T_1 , T_2 , and T_3 states multiplied by the sign of the second Hessian eigenvalue (λ_2).

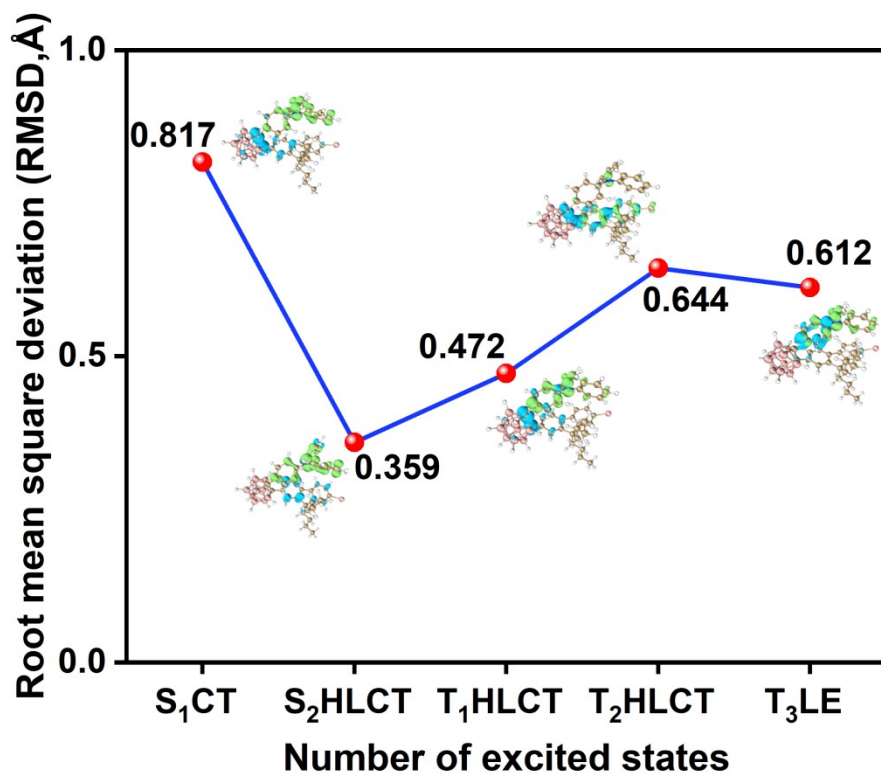


Figure S29. Analysis of root-meansquare deviation (RMSD) vs the different excited structures involved the S_1 , S_2 , T_1 , T_2 , and T_3 states for *o-2*.

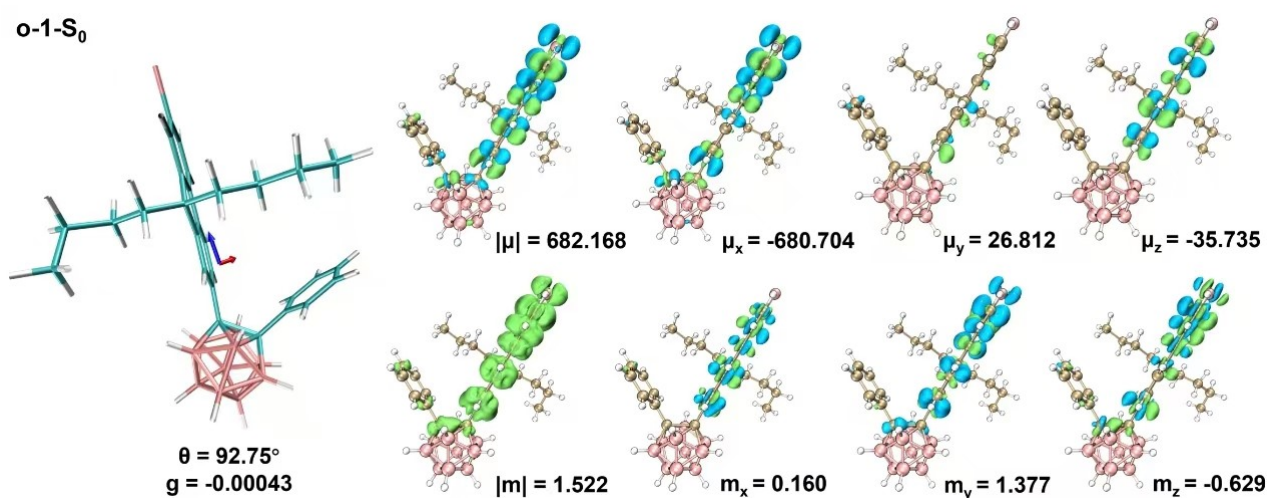


Figure S30. Chemical structure of *o-1* in the ground states (The ETDM vector is marked as blue, and

the MTDM vector is marked as red, θ is the angle between the transition dipole moments). Breakdown analysis of ETDM and MTDM density (isovalue = 0.001) of *o*-1 from Multiwfn and VMD software.

***o*-1-S₁LE**

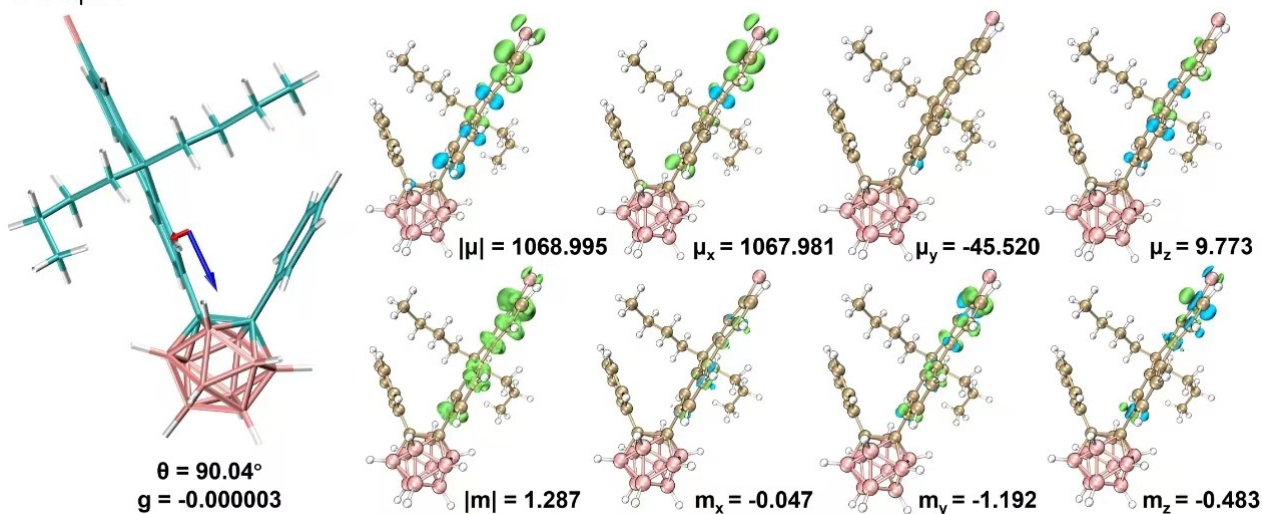


Figure S31. Chemical structure of *o*-1 in the LE states (The ETDM vector is marked as blue, and the MTDM vector is marked as red, θ is the angle between the transition dipole moments). Breakdown analysis of ETDM and MTDM density (isovalue = 0.001) of *o*-1 from Multiwfn and VMD software.

***o*-1-S₁CT**

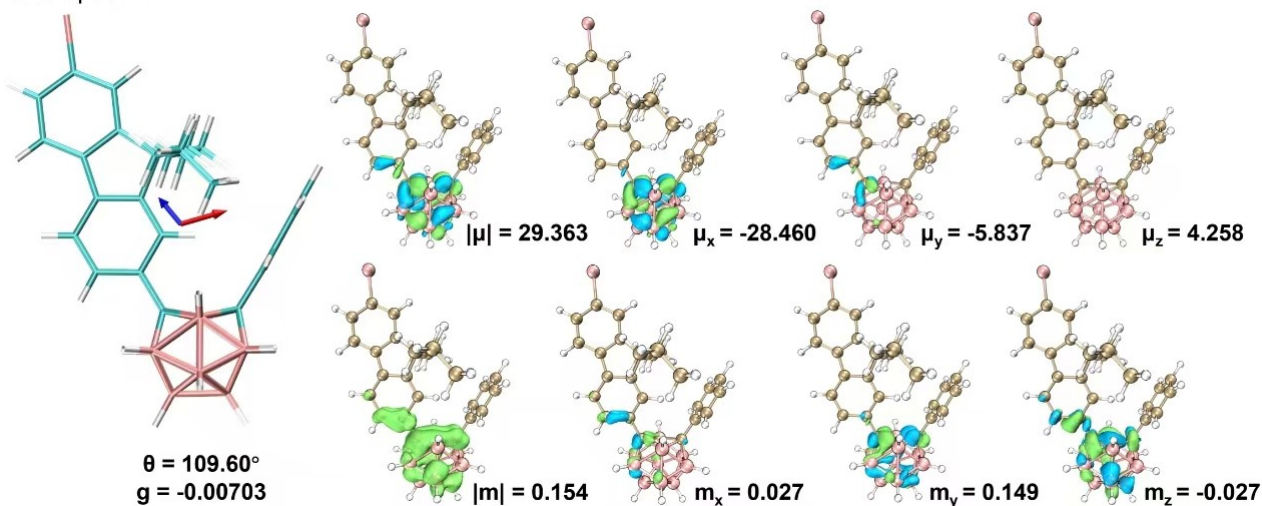


Figure S32. Chemical structure of *o*-1 in the CT states (The ETDM vector is marked as blue, and the MTDM vector is marked as red, θ is the angle between the transition dipole moments). Breakdown analysis of ETDM and MTDM density (isovalue = 0.001) of *o*-1 from Multiwfn and VMD software.

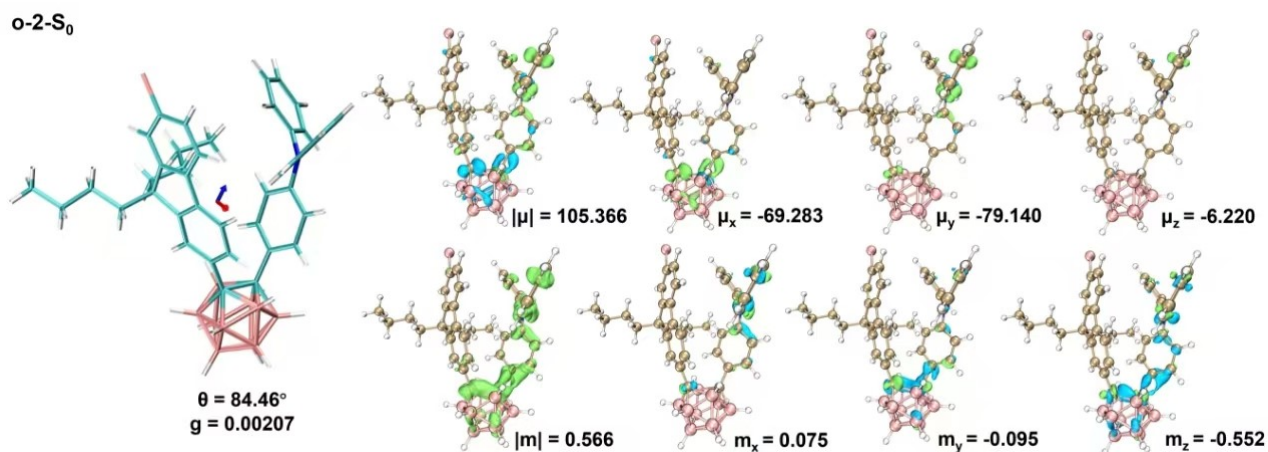


Figure S33. Chemical structure of *o-2* in the ground states (The ETDM vector is marked as blue, and the MTDM vector is marked as red, θ is the angle between the transition dipole moments). Breakdown analysis of ETDM and MTDM density (isovalue = 0.001) of *o-2* from Multiwfn and VMD software.

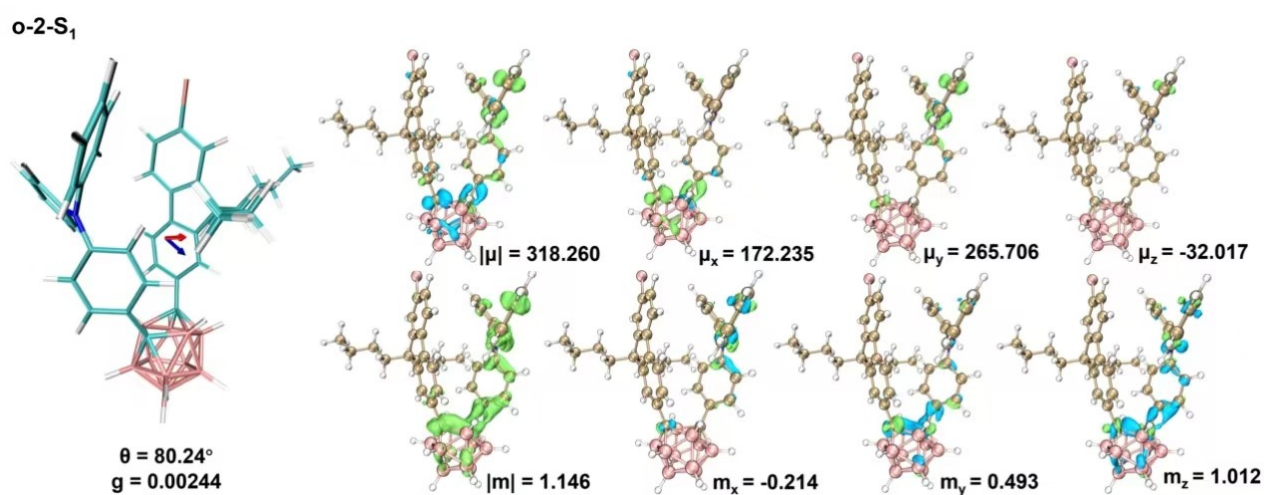


Figure S34. Chemical structure of *o-2* in the CT states (The ETDM vector is marked as blue, and the MTDM vector is marked as red, θ is the angle between the transition dipole moments). Breakdown analysis of ETDM and MTDM density (isovalue = 0.001) of *o-2* from Multiwfn and VMD software.

13. Circular dichroism (CD) spectra

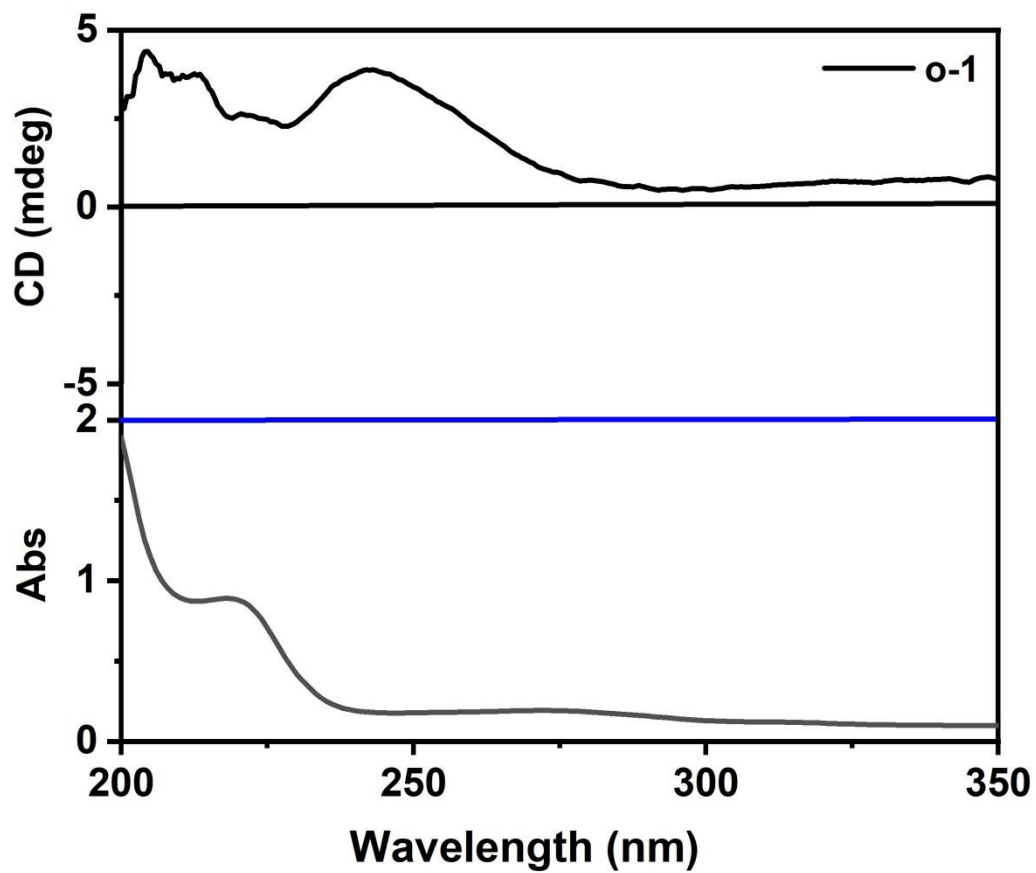


Figure S35. Circular dichroism (CD) spectra of *o*-1 in the methanol suspended emulsion.

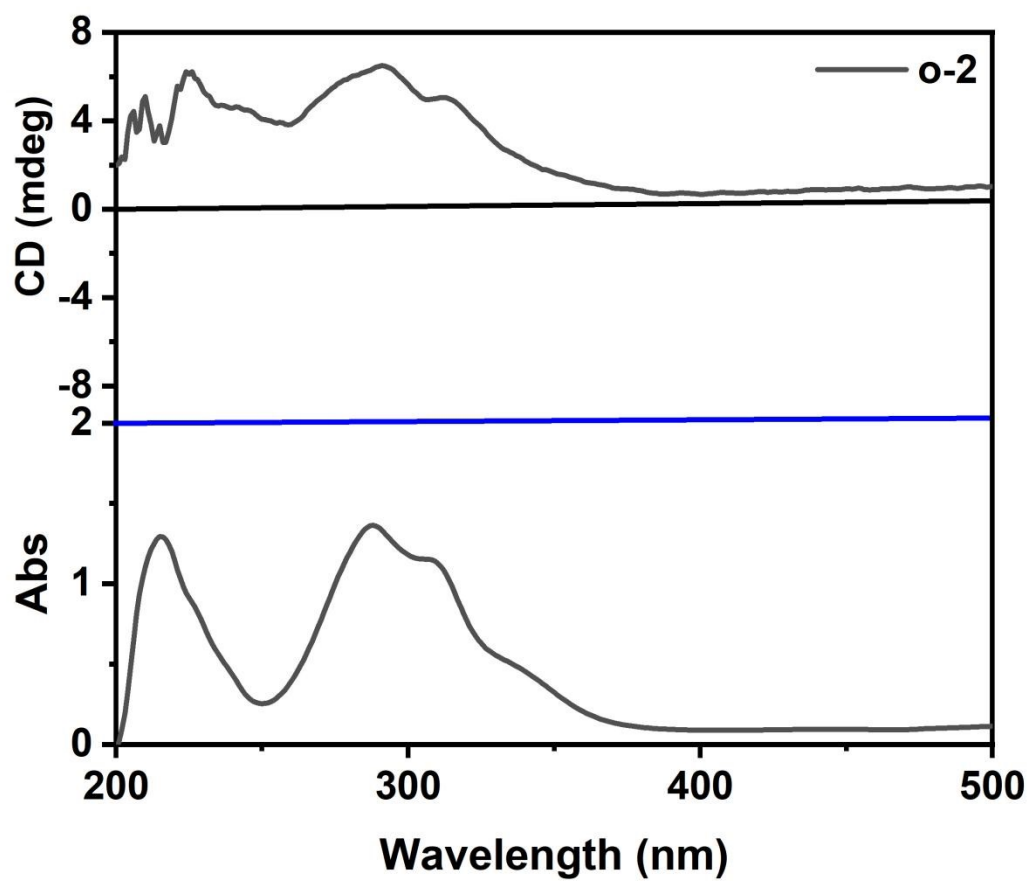


Figure S36. Circular dichroism (CD) spectra of *o*-2 in the methanol suspended emulsion.

14. Raman spectra in the solid states

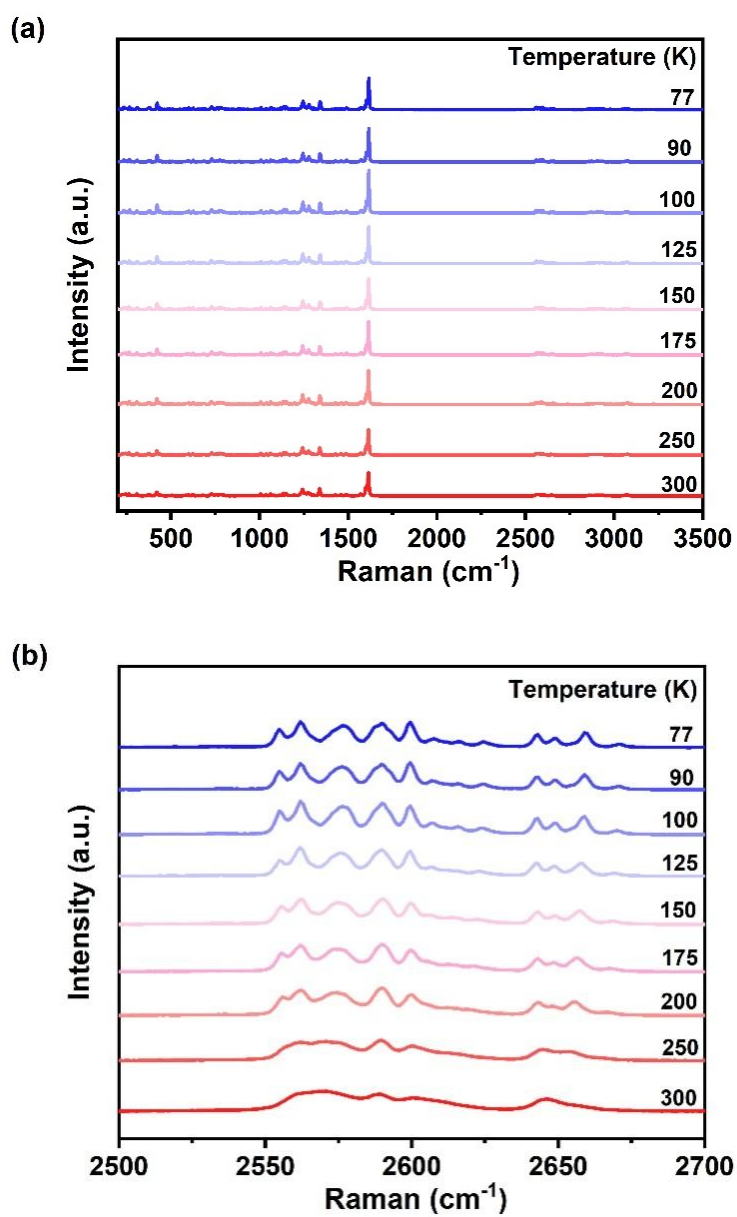


Figure S37. Raman spectra of *o*-1 in the solid states responding to various temperatures, including 77 K, 90 K, 100 K, 125 K, 150 K, 175 K, 200 K, 250 K, 300 K.

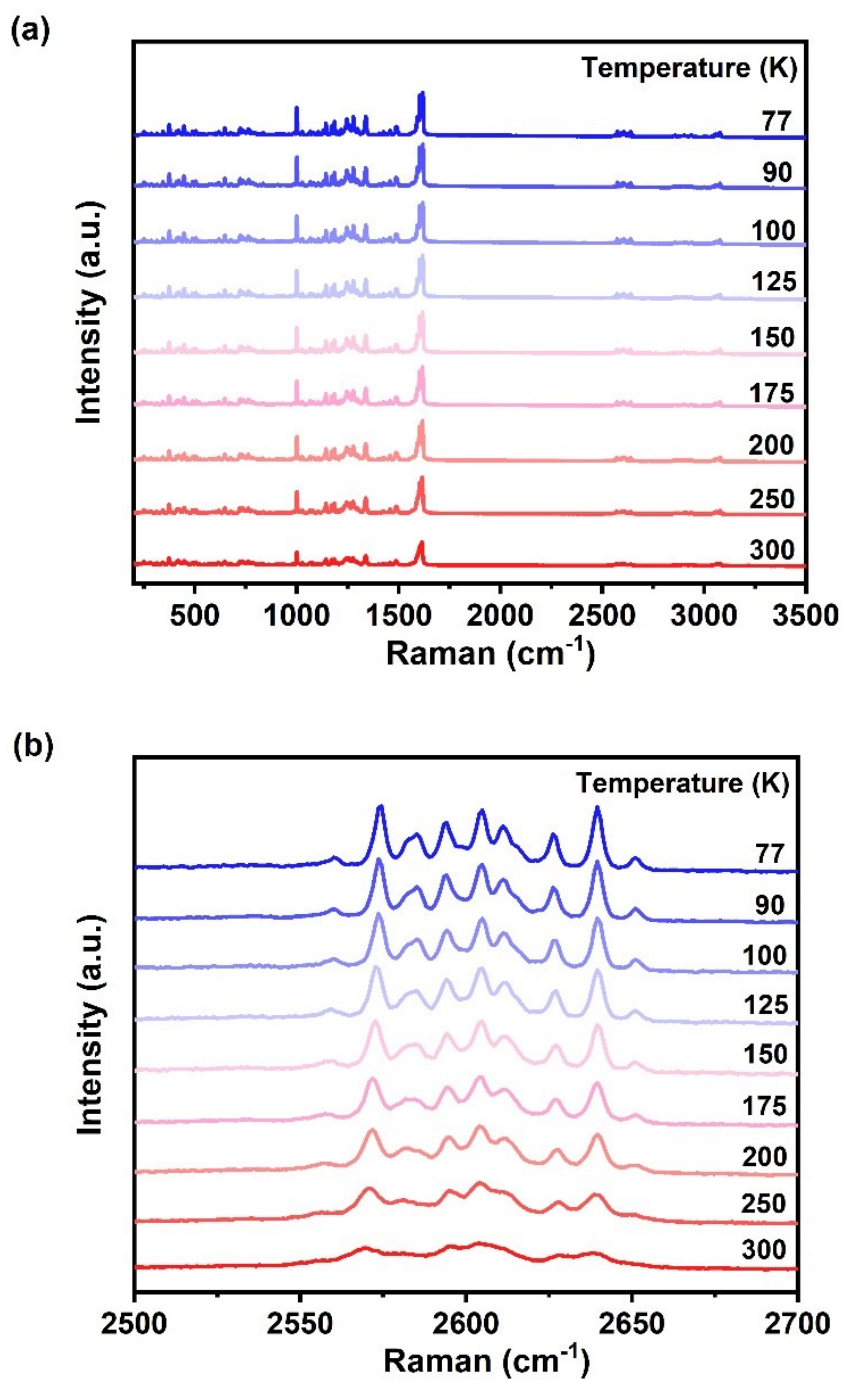


Figure S38. Raman spectra of *o*-2 in the solid states responding to various temperatures, including 77 K, 90 K, 100 K, 125 K, 150 K, 175 K, 200 K, 250 K, 300 K.

15. Emission mechanism

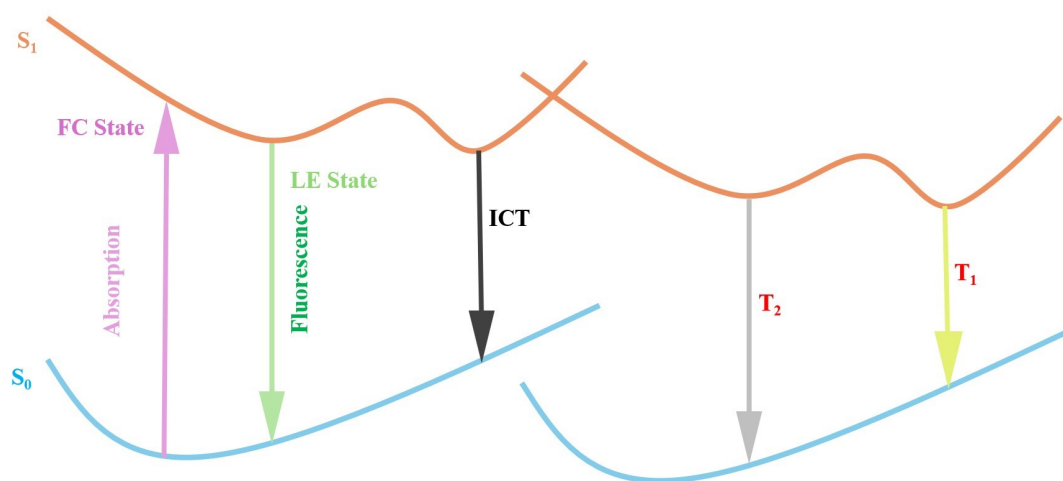


Figure S39. Mechanistic illustration of emissions pathways for molecules *o-1* and *o-2*.

References

1. M. J. Frisch, G. W. Trucks, H. B. Schlegel, G. E. Scuseria, M. A. Robb, J. R. Cheeseman, G. Scalmani, V. Barone, G. A. Petersson, H. Nakatsuji, X. Li, M. Caricato, A. V. Marenich, J. Bloino, B. G. Janesko, R. Gomperts, B. Mennucci, H. P. Hratchian, J. V. Ortiz, A. F. Izmaylov, J. L. Sonnenberg, Williams, F. Ding, F. Lipparini, F. Egidi, J. Goings, B. Peng, A. Petrone, T. Henderson, D. Ranasinghe, V. G. Zakrzewski, J. Gao, N. Rega, G. Zheng, W. Liang, M. Hada, M. Ehara, K. Toyota, R. Fukuda, J. Hasegawa, M. Ishida, T. Nakajima, Y. Honda, O. Kitao, H. Nakai, T. Vreven, K. Throssell, J. A. Montgomery Jr., J. E. Peralta, F. Ogliaro, M. J. Bearpark, J. J. Heyd, E. N. Brothers, K. N. Kudin, V. N. Staroverov, T. A. Keith, R. Kobayashi, J. Normand, K. Raghavachari, A. P. Rendell, J. C. Burant, S. S. Iyengar, J. Tomasi, M. Cossi, J. M. Millam, M. Klene, C. Adamo, R. Cammi, J. W. Ochterski, R. L. Martin, K. Morokuma, O. Farkas, J. B. Foresman, D. J. Fox, Gaussian, Inc., Wallingford, CT, Gaussian 16 Rev. C. 01, 2016.
2. T. Lu, F. Chen, *J. Comput. Chem.* **2011**, *33*, 580.
3. F. Neese, Software update: the ORCA program system, version 4.0. *Computational Molecular Science.* **2018**, *8*, e1327.
4. B. A. Heb, C. M. Marian, O. Gropen, *Chem. Phys. Lett.* **1996**, *251*, 365-371.